DISSERTATIONES
SCIENTIAE
MATERIALIS
UNIVERSITATIS
TARTUENSIS
40

MATI KOOK

Photoexcited processes in ionic liquid vapors

DISSERTATIONES SCIENTIAE MATERIALIS UNIVERSITATIS TARTUENSIS
40

DISSERTATIONES SCIENTIAE MATERIALIS UNIVERSITATIS TARTUENSIS
40

MATI KOOK

Photoexcited processes in ionic liquid vapors

UNIVERSITY OF TARTU
Press
1632

This study was carried out at the Institute of Physics, Faculty of Science and Technology, University of Tartu.

The Dissertation was admitted on October 6, 2025, in partial fulfillment of the requirements for the degree of Doctor of Philosophy in Materials Science and allowed for defence by the Scientific Council on Materials Science of the Faculty of Science and Technology of the University of Tartu.

Supervisors: Prof. Vambola Kisand, Institute of Physics, University of Tartu
Dr. Rainer Pärna, Institute of Physics, University of Tartu
Prof. Ergo Nõmmiste, Institute of Physics, University of Tartu

Opponent: Dr. Oksana Travnikova, Sorbonne Université, Laboratoire de Chimie Physique-Matière et Rayonnement, Paris, France

Defence: January 22, 2026 at University of Tartu, Tartu, Estonia

ISSN 2228-0928 (print)
ISBN 978-9908-57-093-8 (print)
ISSN 2806-2574 (pdf)
ISBN 978-9908-57-094-5 (pdf)

University of Tartu Press
www.tyk.ee

ABSTRACT

This thesis explores the electronic structure of selected ionic liquids (ILs) in the vapor phase, focusing on how different anion–cation combinations influence their electronic structure. The ILs were vaporized in high vacuum using an effusion cell. Ultraviolet photoelectron spectroscopy (UPS) and time-of-flight mass spectrometry (TOF-MS) measurements were performed at the new FinEstBeAMS beamline at the MAX IV Laboratory, where the author contributed to the construction and optimization (Paper I).

During the studies of ILs, the first UPS and in some cases TOF-MS spectra of the vapors of more than 10 ionic liquids: [EMIM][OTf], [PYR_{14}][OTf], [EMIM][DCA], [PYR_{14}][DCA], [PYR_{14}][TCM], [PYR_{14}][FSI], [PYR14][PF_6], [S_{222}][TFSI], [P_{4441}][TFSI] and [EMMIM][TFSI] were obtained and published (Paper III–IV). The TOF-MS study on the fragmentation of [EMMIM][TFSI], [EMIM][OTf] and [EMIM][DCA] revealed the presence of interesting hydrogenated and dehydrogenated fragments (Paper II). The electronic structure of [EMIM][DCA] was thoroughly investigated (Paper IV–V). It was shown that [EMMIM][TFSI] and [EMIM][OTf] have similarities in the fragmentation pattern.

CONTENTS

LIST OF PUBLICATIONS

I. Chernenko, K.; Kivimäki, A.; Pärna, R.; Wang, W.; Sankari, R.; Leandersson, M.; Tarawneh, H.; Pankratov, V.; **Kook, M.** ; Kukk, E.; Reisberg, L.; Urpelainen, S.; Käämbre, T.; Siewert, F.; Gwalt, G.; Sokolov, A.; Lemke, S.; Alimov, S.; Knedel, J.; Kutz, O.; Seliger, T.; Valden, M.; Kirm, M.; Huttula, M.; (2021*). Performance and characterization of the FinEstBEAMS beamline at the MAX IV Laboratory.* Journal of Synchrotron Radiation, 28, 1620–1630. DOI: **10.1107/S1600577521006032**.

II. **Kook, M.**; Kuusik, I; Pärna, R.; Käämbre, T.; Kikas, A.; Tõnisoo, A.; Kahk, J. M.; Kivimäki, A.; Reisberg, L.; Kisand, V.; (2022). *Ion fragmentation study of [EMMIM][TFSI], [EMIM][OTf] and [EMIM][DCA] by vacuum ultraviolet light.* International Journal of Mass Spectrometry, 471, ARTN 116732. DOI: **10.1016/j.ijms.2021.116732**.

III. Kuusik, I.; **Kook, M.**; Pärna, R.; Kivimäki, A.; Käämbre, T.; Reisberg, L.; Kikas, A.; Kisand, V.; (2019). *The electronic structure of ionic liquids based on the TFSI anion: A gas phase UPS and DFT study.* Journal of Molecular Liquids, 294, ARTN 111580–111580-5.
DOI: **10.1016/j.molliq.2019.111580**.

IV. Kuusik, I.; **Kook, M.**; Pärna, R.; Kisand, V.; (2021). *Ionic Liquid Vapors in Vacuum: Possibility to Derive Anodic Stabilities from DFT and UPS.* ACS Omega, 6 (8), 5255–5265. DOI: **10.1021/acsomega.0c05369**.

V. Kuusik, I.; **Kook, M.**; Pärna, R.; Kisand, V.; (2023). *Charge transfer and electronic relaxation effects in the photoemission of EMIM-DCA ionic liquid vapor*. Chemical Physics, 572, 111971.
DOI: **10.1016/j.chemphys.2023.111971**.

Author's Contribution

Paper I. The author contributed to the assembly, optimization, and characterization of the FinEstBeAMS beamline, as well as the development of the solid-state branch, particularly by working on the endstation for commissioning. He also participated in preparing the manuscript.

Paper II. The author was responsible for designing and conducting the experiments, analyzing the data, and drafting the initial version of the manuscript.

Paper III. The author designed a sample injection system, carried out the experiments, and contributed to the analysis of the experimental data and the writing.

Paper IV. The author made improvements to the experimental setup and was responsible for performing the experiments. He participated in experimental data analysis and in the preparation of the manuscript.

Paper V. The author was responsible for planning and performing the experiments. He participated in experimental data analysis, in the preparation of the manuscript and prepared figures for publication.

Author's other publications related to the topic, but not included in this thesis

1. Kook, M; Kaur, H; Danilian, D; Rosenberg, M; Kisand, V; Ivask, A.; (2024). *Durability of photocatalytic ZnO-based surface coatings and preservation of their antibacterial effect after simulated wear*. Journal of Coatings Technology and Research. DOI: 10.1007/s11998-023-00868-2.

2. Kaur, H; Rosenberg, M; Kook, M; Danilian, D; Kisand, V; Ivask, A.; (2023). *Antibacterial activity of solid surfaces is critically dependent on relative humidity, inoculum volume and organic soiling*. FEMS Microbes, xtad022. DOI: 10.1093/femsmc/xtad022.

3. Kisand, V; Visnapuu, M; Rosenberg, M; Danilian, D; Vlassov, S; Kook, M; Lange, S; Pärna, R; Ivask, A.; (2022). *Antimicrobial Activity of Commercial Photocatalytic SaniTise™ Window Glass*. Catalysts, 12 (2), ARTN 197. DOI: 10.3390/catal12020197.

4. Kruusma, J; Tõnisoo, A; Pärna, R; Thomberg, T; Kook, M; Romann, T; Kisand, V; Lust, E.; (2021). *The Electrochemical Behaviour of Quaternary Amine-Based Room-Temperature Ionic Liquid N4111(TFSI)*. Catalysts, 11 (11), ARTN 1315. DOI: 10.3390/catal11111315.

5. Kruusma, J; Tõnisoo, A; Pärna, R; Thomberg, T; Kook, M; Romann, T; Kisand, V; Lust, E.; (2021). *The electrochemical behaviour of protic quarternary amine based room-temperature ionic liquid N2210(OTf) at negatively and positively polarized micro-mesoporous carbon electrode investigated by in situ X-ray photoelectron spectroscopy, in situ mass-spectroscopy, cyclic voltammetry and electrochemical impedance spectroscopy methods*. Journal of Electroanalytical Chemistry, 897, ARTN 115561. DOI: 10.1016/j.jelechem.2021.115561.

6. Juvanen, S; Sarapuu, A; Vlassov, S; Kook, M; Kisand, V; Käärik, M; Treshchalov, A; Aruväli, J; Kozlova, J; Tamm, A; Leis, J; Tammeveski, K.; (2021). *Iron-Containing Nitrogen-Doped Carbon Nanomaterials Prepared via NaCl Template as Efficient Electrocatalysts for the Oxygen Reduction Reaction*. ChemElectroChem, 8 (12), 2288–2297. DOI: 10.1002/celc.202100571.

7. Pelimanni, E; Hautala, L; Hans, A; Kivimäki, A; Kook, M; Küstner-Wetekam, C; Marder, L; Patanen, M; Huttula, M.; (2021). *Core and Valence Level Photoelectron Spectroscopy of Nanosolvated KCl.* The Journal of Physical Chemistry A, 4750–4759. DOI: 10.1021/acs.jpca.1c01539.

8. Kooser, K; Käämbre, T; Vestli, M; Joost, U; Urpelainen, S; Kook, M; Bournel, F; Gallet, J; Lust, E; Kukk, E; Nurk, G.; (2020). *Operando high-temperature near-ambient pressure X-ray photoelectron spectroscopy and*

impedance spectroscopy study of Ni–$Ce_{0.9}Gd_{0.1}O_{2-\delta}$ solid oxide fuel cell anode. International Journal of Hydrogen Energy, 45, 25286–25298. DOI: 10.1016/j.ijhydene.2020.06.228.

9. Sibul, R.; Kibena-Põldsepp, E.; Ratso, S.; Kook, M.; Sougrati, M.T.; Käärik, M.; Merisalu, M.; Aruväli, J.; Paiste, P.; Treshchalov, A.; Leis, J.; Kisand, V.; Sammelselg, V.; Holdcroft, S.; Jaouen, F.; Tammeveski, K.; (2020). *Iron- and nitrogen-doped graphene-based catalysts for fuel cell applications*. ChemElectroChem, 7 (7), 1739–1747. DOI: 10.1002/celc.202000011.

10. Teppor, P; Jäger, R; Härk, E; Sepp, S; Kook, M; Volobujeva, O; Paiste, P; Kochovski, Z; Tallo, I; Lust, E.; (2020). *Exploring Different Synthesis Parameters for the Preparation of Metal-Nitrogen-Carbon Type Oxygen Reduction Catalysts*. Journal of The Electrochemical Society, 167 (5), 054513. DOI: 10.1149/1945-7111/ab7093.

LIST OF ABBREVIATIONS

cPGM	collimated light illuminated plane grating monochromator
DFT	density functional theory
EDLC	electric double layer capacitor
EPU	elliptically polarizing undulator
GPES	gas-phase end station.
HF	Hartree-Fock
HOMO	highest occupied molecular orbital
IL	ionic liquid
IPS	inverse photoemission spectroscopy
IR	infrared
Linac	linear accelerator
LUMO	lowest unoccupied molecular orbital
MP2	Møller–Plesset second order perturbation theory
PLES	photoluminescence end station
SSES	solid-state end station
TIY	total ion yield
TOF–MS	time-of-flight mass spectrometry
UHV	ultra-high vacuum
UPS	ultraviolet photoemission spectroscopy
VUV	vacuum ultraviolet radiation
[EMMIM][TFSI]	1-Ethyl-2,3-dimethylimidazolium bis(trifluoromethylsulfonyl)imide
[EMIM][OTf]	1-Ethyl-3-methylimidazolium trifluoromethanesulfonate
[EMIM][DCA]	1-Ethyl-3-methylimidazolium dicyanamide
[EMIM][TFSI]	1-Ethyl-3-methylimidazolium bis(trifluoromethylsulfonyl)imide
[PYR14][TFSI]	1-Butyl-1-methylpyrrolidinium bis(trifluoromethylsulfonyl) imide
[PYR14][OTf]	1-Butyl-1-methylpyrrolidinium trifluoromethanesulfonate
[PYR14][DCA]	1-Butyl-1-methylpyrrolidinium dicyanamide
[PYR14][TCM]	1-Butyl-1-methylpyrrolidinium tricyanomethanide
[PYR14][FSI]	1-Butyl-1-methylpyrrolidinium bis(fluorosulfonyl)imide
[PYR14][PF6]	1-Butyl-1-methylpyrrolidinium hexafluorophosphate
[S222][TFSI]	Triethylsulfonium bis(trifluoromethylsulfonyl)imide
[P4441][TFSI]	Tributylmethylphosphonium bis(trifluoromethylsulfonyl)imide

1. INTRODUCTION

Ionic Liquids (ILs) are generally defined as molten organic salts with a melting point below 100 °C. ILs are composed of organic cations paired with either organic or inorganic anions. In this work, ion pairs are denoted using the notation [CATION][ANION]. In the notation, the commas between side-chain lengths (e.g. [PYR_{14}]) are omitted to make the notation more compact. It should also be noted that ion pairs are referred to as IL molecules by several authors.

ILs have attracted great interest because of their uncommon physicochemical properties such as low melting temperatures, excellent solvation ability, relatively high thermal stability, low vapor pressure, non-flammability, high electrochemical stability, conductivity etc. [1–3]. It is possible to synthesize a vast number of ILs with tailored properties by selecting from a wide variety of available cations and anions. This enables their use in diverse fields such as electrochemistry, nanotribology, synthesis, catalysis, lubrication, green chemistry, and nanotechnology [4]. In most applications ILs are used in liquid form.

Investigations of isolated IL molecules (in the vapor phase) are the simplest and most natural starting point for understanding the electronic structure of ILs in the liquid phase. Because of this, it is necessary to first perform high accuracy gas phase measurements of free ion pairs – the basic building blocks of ionic liquids. It is unrealistic to synthesize and measure the electronic structure of all possible ionic liquids. The theoretical approach may offer an efficient way to find ILs with suitable properties for specific applications [5–7]. However, despite the advancements in computational methods, high-quality experimental data remains essential for validating and refining theoretical calculations. For example, various *ab initio* methods like Density Functional Theory (DFT) have their limitations, for example, they may not always be suitable for weak interactions (e.g., van der Waals forces, hydrogen bonding, π stacking) that are characteristic of some ILs. There are even more reliable methods, such as Møller–Plesset second order perturbation theory (MP2), but these are also more computationally expensive [8].

When experiments of this work were started in 2013, only a small number of experimental publications about the electronic structure of vapors of ILs were available [9–12]. The reason for this was the highly complicated experimental technique required for such experiments. Not every IL is suitable for vapor phase experiments in vacuum. The ILs under investigation must have very low vapor pressure at room temperature and, in addition, must be thermally stable at vaporization temperatures. *E.g.*, in the case of [EMIM][TFSI], the vapor pressure is $6.2*10^{-5}$ mbar at 169 °C and rises to $1.1*10^{-3}$ mbar at 211 °C [13].

To understand the electronic structure of isolated ILs, suitable experimental techniques should be applied. Ultraviolet Photoelectron Spectroscopy (UPS) is the most direct method for investigating the occupied electronic states. A well-known technique for investigating photo-induced dissociation, fragmentation, and intact parent molecules is Time-of-Flight Mass Spectrometry (TOF-MS). TOF-MS enables the use of soft ionization and has a wide mass to charge

measurement range. In addition, TOF-MS results can confirm that the UPS spectra originate from the parent molecule. These methods provide the most reliable results when used together with a light source that allows for tunable photon energy. Synchrotron radiation was chosen for its exceptional versatility (excellent tunability and intensity) [14].

All experiments in the present thesis were performed at the new FinEstBeAMS beamline at the MAX IV Laboratory. The construction and commissioning of the FinEstBeAMS beamline were the result of a seven-year collaborative effort involving Estonian, Finnish, and other Nordic user communities, in which the author of this thesis also actively participated. It is noteworthy that Paper III was the first scientific article, following the building and commissioning contributions, to originate from the FinEstBeAMS beamline.

This thesis is dedicated to investigations of the electronic structure of selected ILs in the vapor phase. I focused on studying the effects of different anion and cation combinations on the electronic structure of ionic liquids and their fragmentation under vacuum ultraviolet radiation (VUV). This study contributed to a deeper understanding of their fundamental properties. The key motivation was to obtain direct experimental information about the electronic structures of free IL ion pairs. These results were compared with *ab initio* electronic structure calculations (MP2, DFT) of the same compounds, to assess the suitability of existing theoretical approaches at describing these unusual systems.

2. OVERVIEW OF THE CURRENT SITUATION IN THE FIELD OF IONIC LIQUIDS

2.1 Ionic liquids and their applications

ILs are increasingly being used in different applications due to their unique properties (see Figure 1).

Figure 1. Applications of ionic liquids across various fields. Figure reproduced under a CC BY 4.0 license from [30].

In electrochemical applications, they are used in metal electrodeposition [15], batteries [16], sensors [17], dye-sensitized solar cells [18], fuel cells [19], thermo-electrochemical cells [20], and supercapacitors [21]. ILs are used as additives in lubricating agents, corrosion inhibitors, surface-active agents [22], plasticizers, shale inhibitors [23]. In extraction and separation processes these compounds are

applied in micro-extraction [24], biomass extraction [25], extraction of flavonoids, dissolution of wood [26], water treatment technologies, and enhanced oil recovery [27]. In chemical applications ILs are applied in organic reactions, nanoparticle synthesis [28], and enzymatic reactions. Industries that use ILs include the food and bioproduct industry, biodiesel production, and the pharmaceutical industry. In analytical applications, they find use in gas chromatography columns, matrices for mass spectrometry, and in high-performance liquid chromatography [29]. ILs are applied as advanced materials in artificial muscles, liquid crystals, and thermal energy storage devices. In environmental protection ILs demonstrate promising results in carbon capture, the treatment of nuclear waste, and fuel purification [4].

There is a large variety of ILs, which can be synthesized by combining different organic cations with anions. Moreover, substituent groups can be varied in cations like ammonium, sulfonium, imidazolium, triazolium, pyridinium, phosphonium, pyrazolium, guanidinium etc. Some commonly used anions are tetrafluoroborate $[BF_4]^-$, hexafluorophosphate $[PF_6]^-$, bistriflimide, bis(fluorosulfonyl)imide $[FSI]^-$, iodide, chloride, triflate $[OTf]^-$, acetate, and dicyandiamide $[DCA]^-$ [4, 31]. As an example of this versatility, the length of alkyl side chains in imidazolium cations can be adjusted to tune various properties of ILs, such as ionic conductivity [32], the energy gap between the highest occupied and the lowest unoccupied molecular orbitals (HOMO-LUMO gap) [33], and other physicochemical characteristics [34].

2.2 Research topics and spectroscopy of ionic liquid vapors

Although different properties of ILs are the subject of a large number of articles, information about the electronic structure of IL vapors is still limited. One reason for this was the complicated experimental technique and the level of specific know-how needed for such experiments. Even basic information, like the thermal effusion properties of ILs in high vacuum was published for only a few ILs [35]. Although ILs have very low vapor pressures at room temperature (lower than $1*10^{-6}$ mbar) [35], minor vaporization does still occur at elevated temperatures and gas-phase experiments are possible [3, 9–11]. There were some experimental studies of gaseous ILs using mass spectrometry and infrared (IR) spectroscopy (e.g., [8, 36, 37] and references therein), but detailed studies of IL vapors under ionizing radiation were rather few. Both experimental [9, 11, 38–40] and theoretical [41–44] studies have shown that thermal vaporization of ILs produces mainly isolated ion pairs in high vacuum. UPS experiments on [EMIM][TFSI] suggested that IL vapor is mainly composed of cations and anions as isolated IL molecules that are likely to dissociate after photoionization, producing an intact cation and neutral fragments of the anion [9]. Ion pairs have also been directly observed by field ionization [40] and indirectly by soft-ionization mass spectrometry [11, 45], line-of-sight mass spectrometry [38, 46] and UV spectroscopy [9,

12, 47, 48]. UPS and inverse photoemission spectroscopy (IPS) have been used to determine the HOMO and LUMO energy levels of IL droplets [33].

Since the start of our research about ionic liquids in 2013, every year several new publications about gas phase ionic liquids X-ray photoelectron spectroscopy (XPS), UPS and MS are published [24, 49–54]. *In situ* XPS was used to track the evolution of X-ray irradiation-induced chemical reactions in a series of ionic liquids ($[C_nMIM][AuCl_4]$; n=4, 6, 8, 10) on the Si (111) single-crystal surface. [49]. Ambient-pressure XPS was used to examine the impact of water on values of the electrochemical shift C 1s, O 1s and N 1s for [EMIM][OAc] [50]. Ionic liquid-dispersive micro-extraction and detection by high-performance liquid chromatography-electrospray ionization mass spectrometry for antifouling biocides in water was developed [24].

In this thesis, a particular focus was on the characterization of ILs that are being investigated for use in Electrical Double-Layer Capacitors (EDLCs), also known as supercapacitors. Commonly used cations for EDLCs are e.g. $[EMIM]^+$, $[PYR_{14}]^+$, $[DEME]^+$, $[P_{2224}]^+$ and anions are e.g. $[BF_4]^-$, $[PF_6]^-$, $[FSI]^-$, $[TFSI]^-$ [55]. In these systems, ILs are used as the liquid electrolytes. The capacitance of an EDLC is directly affected by the electrochemical stability window and the dielectric constant of the ionic liquid that is used. In turn – these properties are first and foremost governed by the electronic structures of the constituent cations and anions that form the IL. Therefore, a detailed *quantitative* characterization of the electronic structures of free cation-anion pairs – the building blocks of bulk ILs – is of great practical as well as fundamental interest. A full list of the ILs investigated in this thesis, together with figures showing their chemical structures, is presented in Table 1.

3. RESEARCH TASK

3.1 Motivation and formulation of the research tasks

Several ILs have unique properties that are used in specific applications (listed in section 2.1.). As mentioned before, the possible number of anion and cation combinations is huge, and experimentally characterizing all of them is unfeasible [56]. The principal aim of this research project is to perform high accuracy gas phase measurements of free ion pairs – the basic building blocks of ionic liquids. The results of these measurements will be analyzed with reference to theoretical results for the same compounds to gain fundamental insights into the electronic structures of ILs.

The key challenge is to determine the experimental conditions under which such ion pairs can be produced. Indeed, as discussed throughout this thesis, in many cases, heating an IL in vacuum may instead lead to the decomposition of the material.

In turn, this means that it is necessary to experimentally determine the composition of the gas that is released from ionic liquids in vacuum, at room temperature, or at elevated temperatures. This is a nontrivial task that requires a soft ionization and a specialized mass spectrometry setup due to the high molecular masses of the cations and anions involved.

Therefore, in order to be able to perform the experiments described above, and to reach the stated aim of measuring high resolution gas phase photoelectron spectra of ionic liquid vapors, it was first necessary to set up and test the experimental apparatus consisting of an effusion cell, an electron kinetic energy analyzer, and a time-of-flight mass spectrometer, all connected to the analysis chamber at the gas phase endstation of the FinEstBeAMS beamline at the MAX IV synchrotron. The development and commissioning of this experimental setup formed a major part of this research project, which are described in detail in Paper I.

3.2 Statements presented for defense

1. It has been shown conclusively that it is possible to experimentally determine the electronic structure (Paper III–V) and fragmentation patterns of IL vapors (Paper II). This is not trivial, since several experimental parameters and requirements for the IL have to be considered.
2. It was determined that most ILs studied in this work vaporize predominately as isolated ion pairs during heating in vacuum. (Paper II–V)
3. It has been shown that in the case of [EMIM][DCA], there are strong indications that an uncommon interionic charge transfer electronic relaxation process during photoemission occurs. (Paper V)

4. In some cases ([PYR_{14}][FSI], [PYR_{14}][TCM]) indirect experimental evidence of the specific conformer structure of the vaporized species has been obtained. This was possible due to the sensitivity of the UPS spectrum on the underlying ion-pair structure. (Paper IV)
5. The acquired experimental data enabled the reinterpretation of the HOMO energy of [EMIM][BF_4]. The binding energy of the [EMIM][BF_4] ion pair HOMO is now estimated to be 9.25–9.3 eV instead of 7.4 eV. This is suggested by overall agreement with our calculation trends. (Paper IV)
6. The presence of hydrogenated and dehydrogenated fragments was confirmed in [EMMIM][TFSI], [EMIM][OTf] and [EMIM][DCA] (Paper II).

4. EXPERIMENTAL METHODS

4.1 Sample preparation and evaporation

In the present thesis the following ionic liquids were investigated: [EMMIM][TFSI], [EMIM][OTf], [EMIM][DCA], [EMIM][TFSI], [PYR_{14}][TFSI], [PYR_{14}][OTf], [PYR_{14}][DCA], [PYR_{14}][TCM], [PYR_{14}][FSI], [PYR_{14}][PF_6], [S_{222}][TFSI], [P_{4441}][TFSI], [DEME][TFSI] (see Table 1 for chemical and structural formulas). These samples were purchased from IoLiTec Ionic Liquids Technologies GmbH (Germany) or Sigma-Aldrich (USA) and were used as received.

The main motivation for selecting the ILs in (Paper II) ([EMMIM][TFSI], [EMIM][DCA], [EMIM][OTf]) was based on our hypothesis that different anions influence the fragmentation patterns of the same or similar cations, which needed to be confirmed or disproved. As part of the studies, to separately investigate the influence of the anions and the cations on the properties of free ion pairs, two series of ILs were considered. In the first series – [EMMIM][TFSI], [EMIM][DCA], [EMIM][OTf] – the anion is varied, whilst the cation is kept the same (or similar). Experimental measurements of this series of ILs are presented in Paper II. In the second series (Paper III) – [EMIM][TFSI], [DEME][TFSI], [PYR14][TFSI] – the cation is varied, while the anion is kept the same. In (Paper IV) a diverse set of ILs [EMIM][OTf], [PYR_{14}][OTf], [EMIM][DCA], [PYR_{14}][DCA], [PYR_{14}][TCM], [PYR_{14}][FSI], [PYR_{14}][PF_6], [S_{222}][TFSI], [P_{4441}][TFSI], and [EMMIM][TFSI] were chosen for the study. The selection included simple sulfonium- and phosphonium-based cations, aromatic cations like $[EMIM]^+$, non-aromatic rings like pyrrolidinium; and small anions such as $[PF_6]^-$, medium-sized anions like $[FSI]^-$, $[OTf]^-$ and large anions like $[TFSI]^-$.

For each sample transfer, the experimental station was vented with nitrogen (99.995 %), and the effusion cell was removed. The IL sample was poured into a clean quartz crucible under a fume hood and was covered with aluminium foil. The quartz crucible containing the IL sample was transported to the experimental station and inserted into the effusion cell. The effusion cell was then reattached to the experimental station. Pre-vacuum pumping was started through a restricted by-bass valve while degassing intensity was monitored through an inspection port. The estimated ambient air exposure time was approximately 10 minutes for all samples.

Most ILs are known to be hygroscopic to varying degrees [57]. Dissolved water and gases in ILs can be volatile during heating in a vacuum. Vacuum heating at 80–130 °C (depending on the IL) was performed for several hours to remove these unwanted impurities prior to measurement. Uncontrollable volatile out-gassing during operation can potentially damage the experimental equipment. Even small pressure spikes will cause artifacts in both the photoelectron emission and mass spectra. To mitigate this risk, the temperature was gradually increased to 80 °C while continuously monitoring the vacuum pressure gauge for pressure spikes due to outgassing with high-voltage instruments turned off. Pressure spikes caused by water evaporation were visually confirmed to result from outgassing

of the IL. Gas bubbles were observed emerging from the IL. The frequency and amplitude of the pressure spikes during heating depended on the IL. [EMIM][DCA], [PYR_{14}] [TFSI] and [EMMIM][TFSI] showed very little outgassing, while [EMIM][OTf] exhibited pressure spikes two orders of magnitude higher, occurring every 10 seconds even at room temperature. [EMIM][OTf] was left to outgas overnight, the next day no further outgassing was observed, and the vacuum had stabilized. It is important to note that for some ILs, thermal degradation takes place even below the evaporation temperature, however this was not the case with the ILs studied in this work.

The TOF-MS (Paper II) and UPS (Paper III) measurements were carried out in the 10^{-7} mbar pressure range with a liquid nitrogen-cooled cold trap installed on the opposite side of the effusion cell. For UPS measurements in (Paper IV–V), a large turbomolecular pump (400 L/s) was used instead of the liquid nitrogen cold trap, and the same 10^{-7} mbar pressure range was achieved. A schematic illustration of the experimental setup is shown in Figure 2.

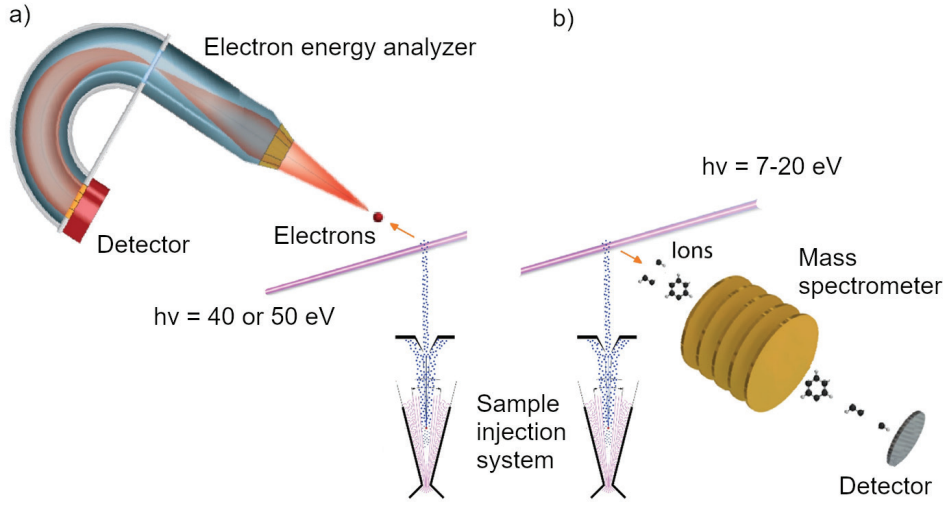

Figure 2. Principal scheme of a) gas-phase XPS and b) TOF measurement setup.

Table 1. Ionic liquids, investigated in the current thesis and [EMIM][BF_4], which is referenced often.

Abbreviation	Chemical formula	Structural formula
[EMMIM][TFSI]	1-Ethyl-2,3-dimethylimidazolium bis(trifluoromethylsulfonyl)imide	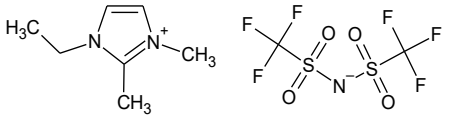
[EMIM][OTf]	1-Ethyl-3-methylimidazolium trifluoromethanesulfonate	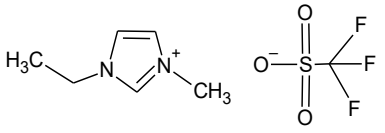
[EMIM][DCA]	1-Ethyl-3-methylimidazolium dicyanamide	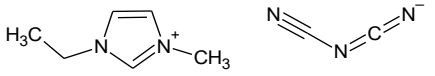
[EMIM][TFSI]	1-Ethyl-3-methylimidazolium bis(trifluoromethylsulfonyl)imide	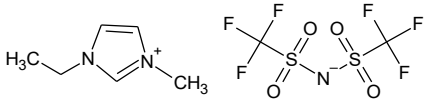
[PYR_{14}][TFSI]	1-Butyl-1-methylpyrrolidinium bis(trifluoromethylsulfonyl)imide	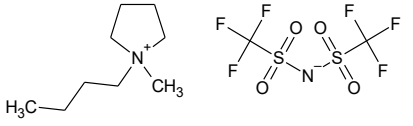
[PYR_{14}][OTf]	1-Butyl-1-methylpyrrolidinium trifluoromethanesulfonate	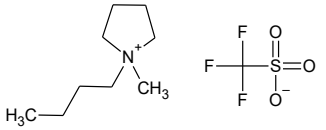
[PYR_{14}][DCA]	1-Butyl-1-methylpyrrolidinium dicyanamide	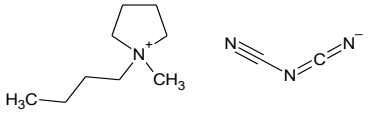
[PYR_{14}][TCM]	1-Butyl-1-methylpyrrolidinium tricyanomethanide	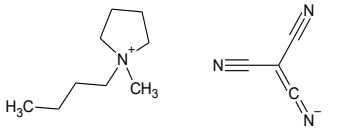
[PYR_{14}][FSI]	1-Butyl-1-methylpyrrolidinium bis(fluorosulfonyl)imide	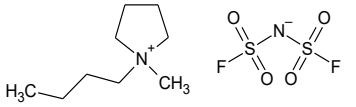
[PYR_{14}][PF_6]	1-Butyl-1-methylpyrrolidinium hexafluorophosphate	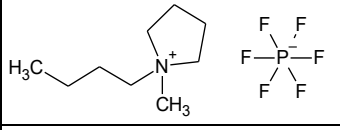
[S_{222}][TFSI]	Triethylsulfonium bis(trifluoromethylsulfonyl)imide	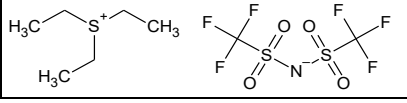

Abbreviation	Chemical formula	Structural formula
$[P_{4441}][TFSI]$	Tributylmethyl-phosphonium bis(trifluoromethyl-sulfonyl)imide	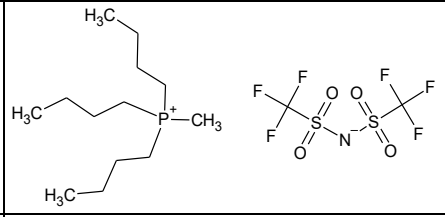
[DEME][TFSI]	Diethylmethyl(2-methoxyethyl)ammonium bis(trifluoromethylsulfonyl)imide	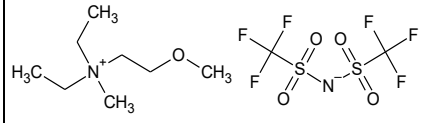
$[EMIM][BF_4]$	1-Ethyl-3-methylimidazolium tetrafluoroborate	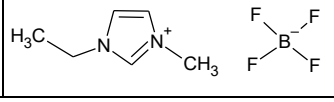

4.2 Time-of-Flight Mass Spectrometry

In traditional photoionization mass spectrometry, the neutral molecules are ionized by Vacuum Ultraviolet (VUV) photons:

$$M + h\nu \rightarrow M^{\bullet +} + e^{-} \quad (1)$$

Here, M is the molecule under investigation and $M^{+\bullet}$ is called the molecular ion or parent ion. Very often, the parent ion is unstable, and it usually fragments into smaller pieces. Uncharged free radicals and neutral molecules will not produce a peak on the mass spectrum. Only charged particles can be detected by the TOF-MS. [58]

When a vapor phase IL ion pair is irradiated by VUV photons, there are two main mechanisms that can produce intact cations $[C]^+$. The first process is the photoexcitation of the IL, followed by the possible dissociation to an intact cation and anion:

$$[C][A] + h\nu \rightarrow [C][A]^{*} \rightarrow [C]^{+} + [A]^{-} \quad (2)$$

The second mechanism is the photoionization of the ion pair, which generates intact cations by dissociation:

$$[C][A] + h\nu \rightarrow [C]^{+} + [A] + e^{-} \quad (3)$$

Since both of these mechanisms also generate various other ions resulting from fragmentation (Paper II) [59], TOF-MS is an excellent experimental method to study these processes.

A schematic illustration in Figure 3 shows the principle of operation of a TOF-MS used in this work. The cations are extracted from the interaction area (E_s) by an electric field pulse, which is also the start time of the time of flight. These cations are then accelerated towards the drift tube by an electric field in (E_d). All cations will acquire the same kinetic energy, which means that the mass distribution of cations will result in a distribution of their velocities. The distance traveled in the field-free drift tube (D) results in a distribution of flight times.

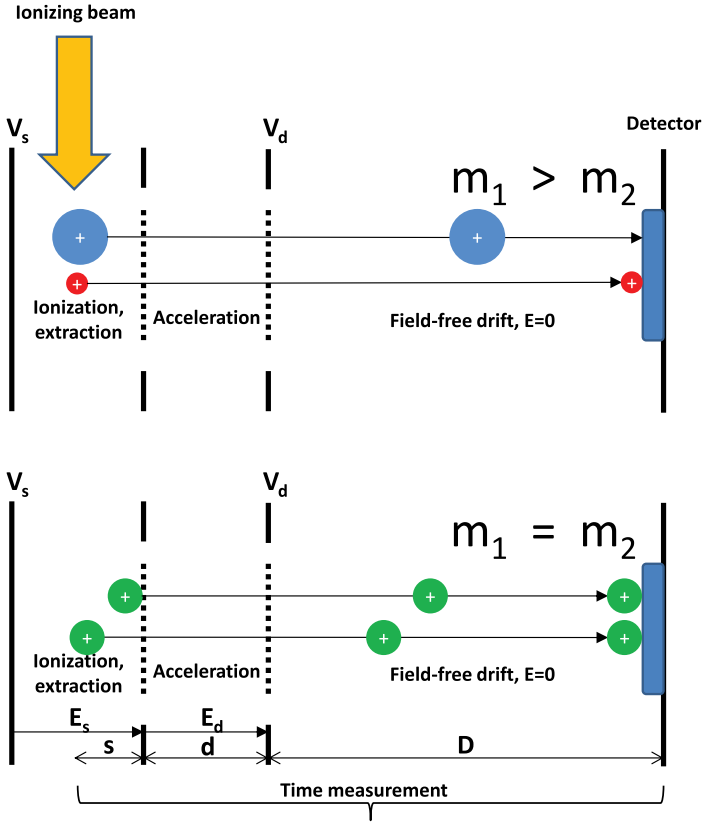

Figure 3. Schematic illustration of a Time-of-flight Mass Spectrometer. Top: Ions with different masses but the same initial position arrive at the detector at different times. Bottom: Ions with the same mass and different initial positions arrive at the detector simultaneously, demonstrating space focusing. Courtesy of Marta Berholts. [60]

In principle, the upper mass range of a time-of-flight instrument has no limit, which makes it especially suitable for soft ionization techniques. Another advantage of these instruments is their high transmission efficiency, which leads to very high sensitivity. The analysis speed of TOF analyzers is very fast, and a spectrum over a broad mass range can be obtained in microseconds. So, it is possible in theory to produce in 1 second several thousand TOF mass spectra over a very wide mass range. But in practice, for most of the applications, the small number of ions detected in each individual spectrum is insufficient to provide the

required precision of mass or abundance measurement. Furthermore, it is actually impossible to record all these individual spectra one by one at such a rate without exceeding the speed of data transfer and the capacity of data storage of most computers. Thus, recorded spectra are generally the addition of a number of individual spectra. [58]

Another interesting characteristic of the TOF analyzer lies in its easy mass calibration with only two reference points. The TOF mass spectrometer requires a calibration equation to convert the measured ion flight times into mass-to-charge values [58]. The time of flight, T, of an ion is directly proportional to the square root of the ion's m/z and is expressed as:

$$T = T_0 + C\sqrt{\frac{m}{z}} \tag{4}$$

where T_o and C are calibration constants that depend on the parameters of the spectrometer and could be calculated by solving the above equation for two known mass signals (e.g. rest gas ions always present in the vacuum chamber such as N_2^+ and H_2O^+). The typical flight times of the ions are in the order of microseconds [60]. The calibration is more accurate if the calibrant peaks are far apart from each other [58].

4.3 Photoelectron spectroscopy in the gas phase

An intense beam of ultraviolet light (in this work, 40 and 50 eV was used) ionizes molecules of a gas in a vacuum. This energy is sufficient to ionize electrons from the valence shell, which are involved in chemical bonding. Electrons have a characteristic binding energy, the minimum energy needed to eject them to infinity. Part of the photon's energy is used to overcome this binding energy and the rest must appear as kinetic energy of the ejected electrons. An illustration of photoionization and photoexcitation is shown in Figure 4.

The ejected electrons are separated according to their kinetic energies in an electron analyzer, detected and recorded. The photoelectron spectrum is a record of the number of electrons detected at each energy, corresponding to the binding energy of an electron in an atom.

There are several mechanisms that broaden the lines observed in the UPS spectra. Here are outlined some important ones:

1. Photoionization generally changes the potential energy surfaces of the molecule (IL) and the new vibronic progressions leave a corresponding energy change to the photoelectron energy leading to vibronic broadening.
2. At finite temperatures, molecules populate higher vibrational and rotational states, which leads to thermal line broadening.
3. The finite lifetime of the ionized state introduces uncertainty in the energy of the emitted electron, leading to lifetime broadening

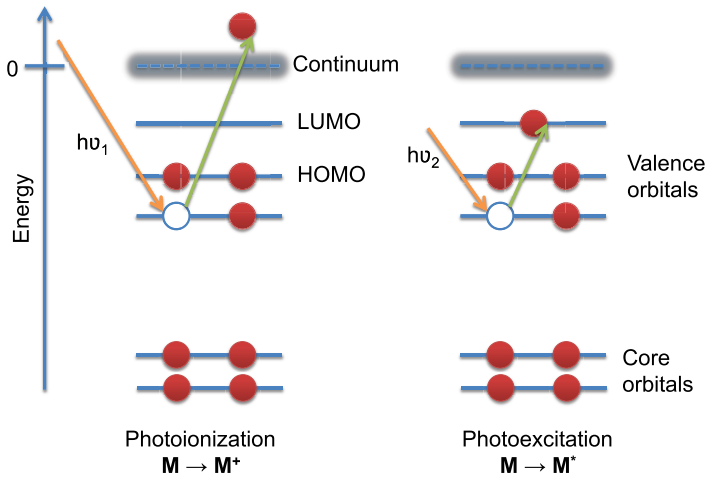

Figure 4. Left: Schematic of the photoelectric effect during UPS. A valence electron is ejected by an incident ultraviolet radiation from its valence band. Right: At lower incident radiation energies than is required for ejecting a valence electron into a continuum, photo-excitation can occur. Courtesy of Marta Berholts. [60]

4.4 *Ab initio* calculations

Publications III, IV and V contain besides experimental results also theoretical calculations. Although these calculations are not performed by the author of the present thesis, some comments are given below about the theoretical methods used.

Density Functional Theory (DFT) and Hartree-Fock (HF) are both methods used in computational quantum chemistry to calculate the electronic structure of atoms and molecules. Both belong to the family of first principles (*ab initio*) methods, so named because they can predict material properties for unknown systems without any experimental input.

In DFT, the functional is the electron density, which is a function of space and time. The electron density is used in DFT as the fundamental property. HF considers the wavefunction of each electron individually. Another key difference between DFT and HF is the way that they treat electron correlation. In DFT, electron correlation is treated using an exchange-correlation functional, which is a mathematical approximation of the many-body effects of electron correlation. HF currently does not treat correlation, but the perturbation theory (post-HF) is able to add some elements of the correlation.

Hybrid functionals are a class of approximations to the exchange–correlation energy functional in DFT that incorporate a portion of exact exchange from Hartree–Fock theory with the rest of the exchange–correlation energy from other sources (*ab initio* or empirical).

Møller–Plesset perturbation theory (MP) is one of post-Hartree–Fock *ab initio* methods. It improves on the HF method by adding electron correlation effects by means of Rayleigh–Schrödinger perturbation theory (RS-PT), usually to second (MP2), third (MP3) or fourth (MP4) order.

4.5 Synchrotron radiation generation

The working principle of a synchrotron relies on the fact that accelerating charged particles (electrons or positrons) close to the speed of light emit electromagnetic radiation with a small natural divergence [61]. A schematic illustration of a typical synchrotron is presented in Figure 5. A modern synchrotron facility consists of 4 main components held under ultra high vacuum (UHV) to minimize electron collisions with the rest gas molecules and to prevent absorption of the produced radiation. These components are discussed below with a short description of processes happening to the electrons and the emitted electromagnetic radiation.

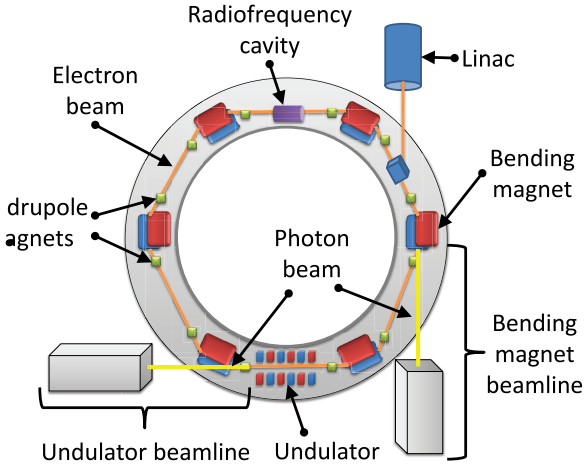

Figure 5. Schematic illustration of a synchrotron storage ring. Courtesy of Marta Berholts. [60]

4.5.1 Linear accelerator

The linear accelerator (Linac) accelerates electrons generated in the electron gun with high voltage. Linac incorporates an electron gun at one end (the cathode), and as the electrons are emitted, they are directed to the positive anode located on the opposite end. In the center of the anode is a small aperture, followed by a transfer line, that allows the electrons to pass through either into the booster ring that accelerates the electron stream even further to the energy of electrons in the main storage ring or less (commonly measured in GeV) or straight to the storage ring via transfer line.

4.5.2 Storage ring and insertion devices

The storage ring stores the relativistic electrons inserted from the Linac or the booster ring. Around the storage ring, there are different kinds of magnets, which force the electron beam to focus (quadrupole magnets), to bend (bending magnet),

or to travel in a "snaking" path (undulator, wiggler) illustrated in Figure 6. When relativistic electrons are accelerated perpendicular to their velocity, they emit synchrotron radiation. The radiofrequency cavity supplies the electrons with the required amount of energy to compensate for the energy loss due to emitted radiation when electrons pass the magnetic structures.

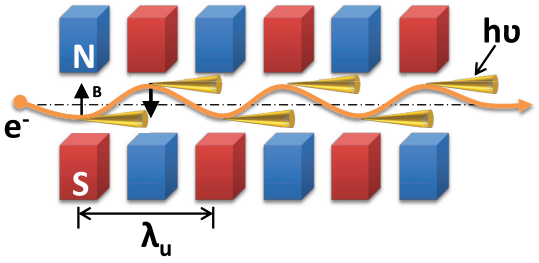

Figure 6. Schematic illustration of an undulator/wiggler. Courtesy of Marta Berholts. [60]

Undulators and wigglers (see Figure 6) are insertion devices that consist of a periodic structure of dipole magnets. The key characteristic of undulators and wigglers is the strength K:

$$K = \frac{eB\lambda_u}{2\pi m_e c} \tag{5}$$

where e is the electron charge, B is the magnetic field, λ_u is the spatial period of the undulator magnets, m_e is the electron rest mass, and c is the speed of light.

In a classic wigglers (K >> 1) electrons radiate independently and a wide high-power spectrum is the result. In general, the wiggler acts like a sequence of bending magnets with alternating polarities. The wiggler spectrum is more intense (equation 6) than the bending magnet.

$$I \propto N_{electrons} \text{ x } N_{poles} \tag{6}$$

$$I \propto N_{electrons} \text{ x } (N_{poles})^2 \tag{7}$$

where $N_{electrons}$ is the number of electrons and Npoles is the number of magnetic poles.

In a classic undulator (K << 1), the magnetic field is weak, and beam deflections are small. This results in radiation interaction with itself, producing destructive and constructive interference and thus intensive radiation (equation 7). The undulator spectrum consists of intense peaks. Insertion devices are placed in straight sections of the storage ring. [62]

4.5.3 Beamlines

The beamlines start after the magnetic structure of insertion devices or bending magnets and run off tangentially from the storage ring. The first part of the beamline is the front end, whose main function is to reduce heat load from the insertion device directed toward the beamline's first mirror and to protect users from unwanted radiation. Beamlines have many optical devices (monochromators, filters, beam-position monitors, mirrors, lenses, etc.) to control and improve the quality of the radiation produced by insertion devices, measuring and purifying the photon beam along its final path to the experimental chamber.

The monochromator is an optical device that separates light/radiation into a wide range of wavelengths or energies. The optical concept behind the plane grating monochromator is described in detail by Petersen [63]. One of the most successful monochromators used at synchrotron beamlines is the plane grating monochromator SX-700 produced by Zeiss [64]. This has been further developed into collimated light plane grating monochromator (cPGM) [65], which is used at FinEstBeAMS. The cPGM concept arises from the fact that although emitted synchrotron radiation is in a very narrow cone, the light is not parallel. Thus, the plane grating would be illuminated with divergent light. This issue has been addressed by introducing an additional optical element (mirror) in front of the monochromator. The mirror works as a collimator to produce parallel light in the dispersion plane of the monochromator. The principle of collimated light allows us to operate in high energy resolution, high flux or high spectral purity mode. [65]

The resolving power of a spectrometer is defined as:

$$R = \frac{\lambda}{\Delta\lambda} \tag{8}$$

Where $\Delta\lambda$ is the spectral resolution of a spectrometer – the minimum wavelength difference that can be distinguished at the wavelength λ.

4.5.4 Experimental end-stations

Experimental end-stations are used to perform the experiments, as here radiation hits the sample placed in its path. Each endstation is designed specifically for the types of experiments conducted on that beamline. In general, each one consists of a sample holder or a sample injection system and a detection system, as well as computers through which the researchers control their experiments and view data as it is recorded.

4.6 Design of the FinEstBeAMS Beamline

The FinEstBeAMS beamline at MAX IV Laboratory (Lund, Sweden) was designed to fulfill the various needs of the Estonian, Finnish, and Nordic user communities in gas-phase electron and ion spectroscopies, surface science and

photoluminescence research, while also providing a modern instrument to any users of synchrotron radiation with their own experimental end stations. Therefore, the beamline had to afford an extensive photon energy range from ultraviolet to soft X-rays, good performance in terms of photon energy resolution and photon flux (often needed in gas-phase electron spectroscopy), reasonably small focal spot sizes to allow moderate spatial resolution in surface studies, and a possibility to probe samples with light of variable polarization. A further restriction in the design was to have only one undulator and one monochromator despite the extended operation range. A solution of how these demanding goals can be achieved was presented in the beamline design paper [66].

The FinEstBeAMS beamline is located at 1.5 GeV storage ring at MAX IV Laboratory and covers a wide photon energy range, 4.3 – 1000 eV, and gives an opportunity to probe core and valence levels with a focused or defocused beam using light, produced by an elliptically polarizing undulator (EPU) with variable polarization. [66]

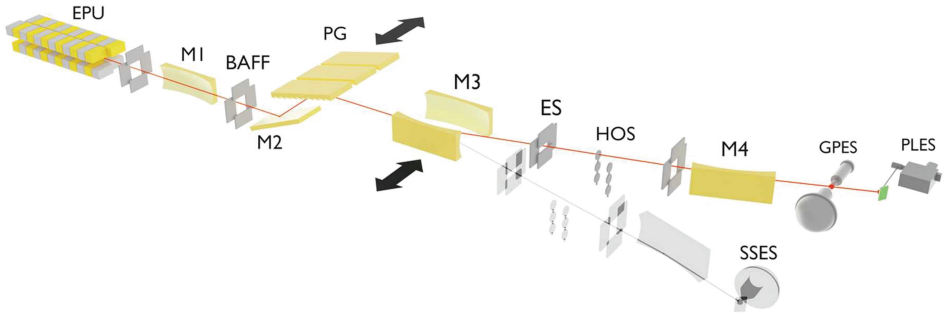

Figure 7. Schematic layout of the beamline optical system. The following abbreviations are used: EPU – elliptically polarizing undulator, M1–M4 – mirrors, BAFF – baffles, PG – plane grating, ES – exit slit, HOS – higher-order suppressing filters, GPES – gas-phase end station, PLES – photoluminescence end station, and SSES – solid-state end station. Figure reproduced under a CC BY 4.0 license from (Paper I).

The EPU of the beamline is based on the APPLE II design with permanent magnets [67]. All four arrays of magnets can be shifted in the longitudinal direction which allows full control of the light polarization. The first undulator harmonic will cover in the circularly polarized mode the photon energy range of 4.9 – 207eV. At higher photon energies higher harmonics have to be used and the degree of circular polarization typically goes down to 70–80%. The undulator has a high K value (10.065), thus when the undulator gap is closed down to 14 mm, its spectrum resembles that of a wiggler at high photon energies (> 1000 eV). In wiggler mode the undulator can reach close to 1500 eV photon energy. This means that experiments are feasible also at 1253 eV and 1486 eV and allow for direct comparison to results obtained using Mg and Al Ka laboratory X-ray sources. Furthermore, running the undulator as a wiggler provides quite high photon flux at high photon energies: at 1000 eV the estimated flux exceeds 10^{12}

ph/sec for 0.1% band width compared to undulator mode, where expected flux is 10^{10} ph/sec for 0.1% band width.

The beamline optical design (Figure 7) was based on cPGM [66]. The pre-mirror is collimating toroidal mirror (M1). The monochromator consists of an internally cooled plane mirror (M2) and two gratings: the first one (PG1), with 600 lines mm^{-1} line density (high ruling), can be used at photon energies from 15 to 1300 eV. The second one (PG2) operates in the photon energy range from 4.5 to 50 eV and has an exceptionally sparse line density of 92 lines mm^{-1} (low ruling). The dispersed radiation from the grating will be focused by two identical, not actively cooled toroidal focusing mirrors at the gas-phase or solid-state branch line exit slits (M3). Switching between the branch lines will be achieved by inserting either of the two focusing mirrors into the beam path (M3). The re-focusing for the gas-phase and solid-state branch-lines will be accomplished by a single ellipsoidal mirror (M4).

The FinEstBeaMS beamline was modeled with the program RAY [68]. First, the resolution predicted by the analytical model was tested by ray tracing. The correspondence was excellent and showed that the resolution is mostly limited by the diffraction limit set by the grating. Thus, the required resolving power (as input of the user community), R=5000–10000 over the whole photon energy range shall be within the reach. A standard way to compare beamlines is to give the flux at a certain resolving power over the photon energy range of the beamline. Figure 8 shows the result of simulations in the case R=5000, a typical setting foreseen for most experiments.

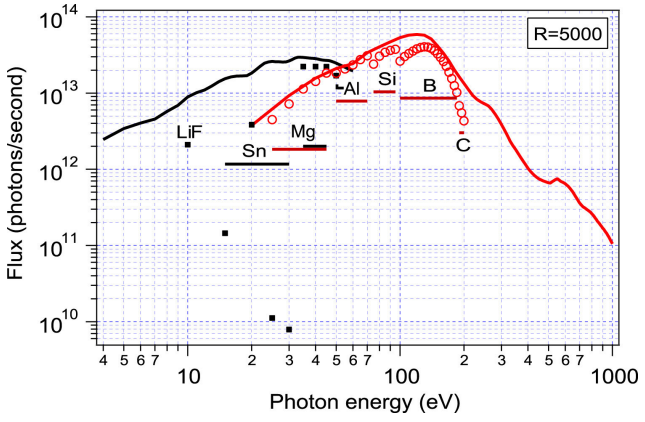

Figure 8. In design phase planned photon flux at experiment for the 92 l/mm grating (curve at left, black colour, photon energies 4.3 to 60 eV) and the 600 l/mm grating (curve at right, red colour, photon energies 60 to 1000 eV) for resolving power of 5000, i.e. 0.02% band width [66]. Beamline acceptance was set at 1 mrad × 0.2 mrad, and it was assumed that the most efficient undulator harmonic is tuned for each photon energy. A ring current of 500 mA was used in these calculations. Solid squares and open circles show the first order flux for the two gratings after using filters of 200 nm thickness under the condition that the sum of the second and third order flux is 1% or less of the first order flux. Horizontal bars depict the energy ranges of the different filters. Figure reproduced under a CC BY 4.0 license from [66].

FinEstBeAMS has three experimental endstations (see Figure 7): the gas-phase end station (GPES) [69], the solid-state end station (SSES) [70], and the photo-luminescence endstation (PLES) [71].

The experimental work of this thesis was carried out at GPES endstation. The GPES is designed for gas-phase targets and samples with high vapor pressure not suitable for UHV conditions. The main instruments of GPES are a Scienta R4000 electron spectrometer and a Wiley-McLaren TOF-MS. The electron and ion spectrometers can also be used independently for high-resolution electron and ion spectroscopy or to collect electron and ion yields as a function of photon energy. The GPES is portable and allows to connect user designed equipment, like the effusion cell that was designed and used to vaporize ionic liquids in the present work.

5. RESULTS AND DISCUSSION

5.1 Paper I – Performance and characterization of the FinEstBeAMS beamline at the MAX IV Laboratory

Construction of a beamline in a synchrotron facility is a long process where numerous people spend tens of thousands of working hours together. Publication[I] is a summary of this enormous work, which gives a strong backbone for all further scientific works that have already been performed and will be performed in the future at the FinEstBeAMS beamline. While publication [66] reflected the design and expectations for the beamline in the planning phase, (Paper I) reports the actual performance of the operational beamline.

The photon energy resolution of the beamline is one of the most important parameters for every beamline. In the (Paper I) this was investigated by measuring the Total Ion Yield (TIY) spectra of several gases at the GPES. For that purpose, the Ne 1s → 3p, Ne 2p → 13d, N_2 N 1s → π*, Ar $2p_{3/2}$ → 4s, and Xe $5p_{1/2}$ → 9s resonances were used. To give a visual demonstration of the spectral resolution, Ne 2p → nd, ms spectra are displayed in Figure 9.

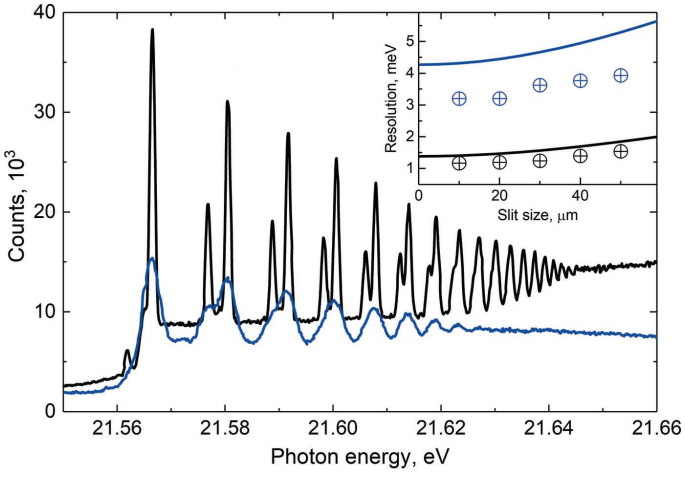

Figure 9. TIY spectra of Ne 2p → *nd, ms* excitations measuring using the 600 lines mm^{-1} grating (black line) and 92 lines mm^{-1} grating (blue line) measured with 10 μm exit slit. (Inset) Experimentally obtained (dots) and calculated (solid lines) dependencies of resolution of the slit widths for the corresponding graph. Figure modified under a CC BY 4.0 license from (Paper I).

The Ne 2p and Xe 5p excitation spectra were approximated by the Gaussian functions, as the contribution of lifetime in the widths of these spectra was assumed to be negligible.

Photon energy resolution of the beamline was estimated by taking into account four main factors: source size, exit slit width, slope errors of the optical elements and the diffraction limit. For the sake of simplicity, it was assumed that all of

these factors follow a Gaussian distribution. Thus, quadratic summing can be used to estimate the overall resolution.

In this way, it is possible to estimate the photon energy resolution in a wide energy range and with different values of slit widths (Figure 10). The calculated values are expected to reproduce well the experimental resolution, apart from a slight overestimation in the low-energy range. In Figure 10, dash-dotted lines are shown as eye-guides for values of constant resolving power.

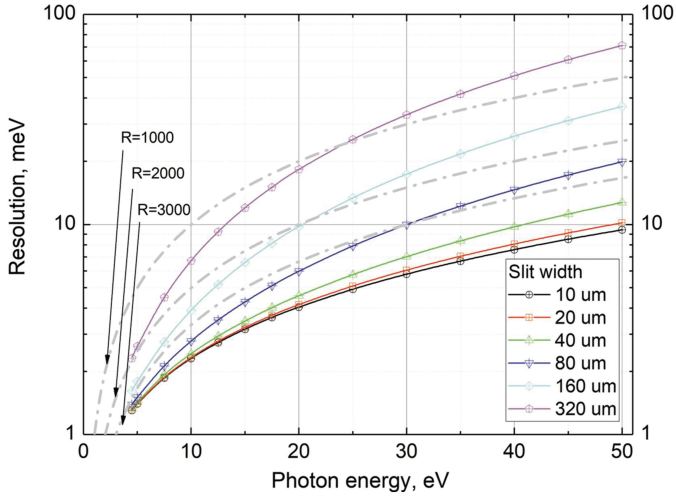

Figure 10. Calculated photon energy resolution for the 92 l/mm grating. Corresponding values of slit width are shown in the plot legend. Gray dashed lines show values of constant resolving power. Figure reproduced under a CC BY 4.0 license from (Paper I).

The main conclusion of the publication (Paper I) is that the FinEstBeAMS beamline works as designed. The achieved resolution of the beamline is even better than planned because the quality (surface roughness, etc) of gratings is better than expected during the beamline design phase. Experimental data also demonstrate that the beamline flux is slightly weaker than planned, since the first mirror (M1) of the beamline is not collecting photons as well as was expected during the planning phase. Due to M1 inefficient cooling, frontend movable masks are closed down to 0,6x0,8 mm, which limits M1 acceptance more than was initially planned. As expected, the combination of the low-line-density grating and grazing-incidence optics on the beamline results in poor high-order suppression in monochromated light. Therefore, each of the two beamline branches contains specific filter units, where six different filters can be mounted, purifying the radiation further for low photon-energy experiments (Paper I).

The implementation of the FinEstBeAMS beamline was important for European communities in gas-phase electron and ion spectroscopies, surface science, and photoluminescence research, while in Europe, only some beamlines are available in the respective energy region.

5.2 Paper II – Ion fragmentation study of [EMMIM][TFSI], [EMIM][OTf] and [EMIM][DCA] by vacuum ultraviolet light

In (Paper II), the photo-induced fragmentation processes by detecting fragment ions and their varying intensities as a function of VUV photon energy of three different ILs: [EMMIM][TFSI], [EMIM][OTf], and [EMIM][DCA] were studied. The aim of this paper was to identify the fragmentation pathways of $[EMIM]^+$ and $[EMMIM]^+$ cations and to compare the effect of different anions on the photo-fragmentation channels.

The nomenclature for the fragments is derived from the cation notation. The parent ion $[EMMIM]^+$ (1-Ethyl-2,3-dimethylimidazolium) fragments to $[MMIM]^+$ (2,3-dimethylimidazolium), $[MMIM]^{+\bullet}$ (2,3-dimethylimidazolium-1-yl), $[2MIM]^+$ (2-methylimidazolium), $[IM\text{-}H]^{+\bullet}$ (imidazolium-1-yl).

5.2.1 [EMMIM][TFSI]

In the TOF-MS spectra of [EMMIM][TFSI] (Figure 11), only singly charged ions are present (i.e., z=1). This is due to the relatively low photon energies and intensities used for the photoexcitation. The intact $[EMMIM]^+$ cation peak was identified at m/z 125 and the cation fragments were also observed. During the fragmentation of $[EMMIM]^+$ and $[EMIM]^+$ based ILs the aromatic imidazolium ring can remain intact, or it may break. The fragments at m/z 42 ($C_2H_4N^+$) and 54 ($C_3H_4N^+$) result from the breaking of the imidazolium ring, as proposed in [72] and [73].

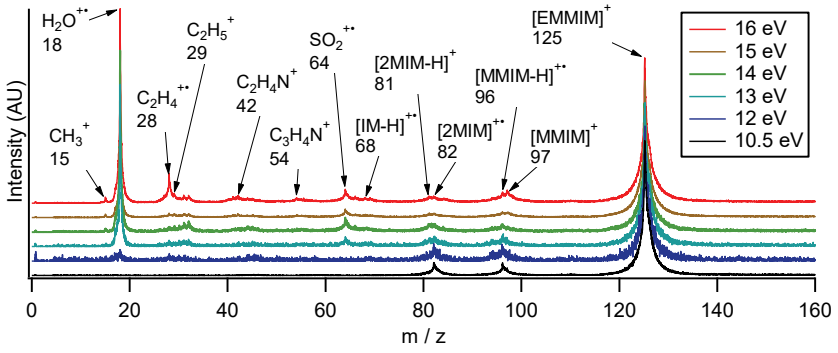

Figure 11. TOF-MS spectra of [EMMIM][TFSI] acquired at different photon energies at the temperature of 200 °C. Excitation photon energies and key fragments are given in the figure (Paper II).

One would expect to observe a fragment at m/z 111 $[EMIM]^+$, because the typical fragmentation pattern for a similar IL, [EMIM][TFSI], involves the loss of the methyl group from the nitrogen position [74]. However, no peak at m/z 111 was detected. It was proposed that fragmentation pathways that involve the loss of the ethyl group are so much more probable than the m/z 111 fragment $[EMIM]^+$ (Paper II).

5.2.2 [EMIM][OTf]

TOF-MS spectra of [EMIM][OTf] are demonstrated in Figure 12.

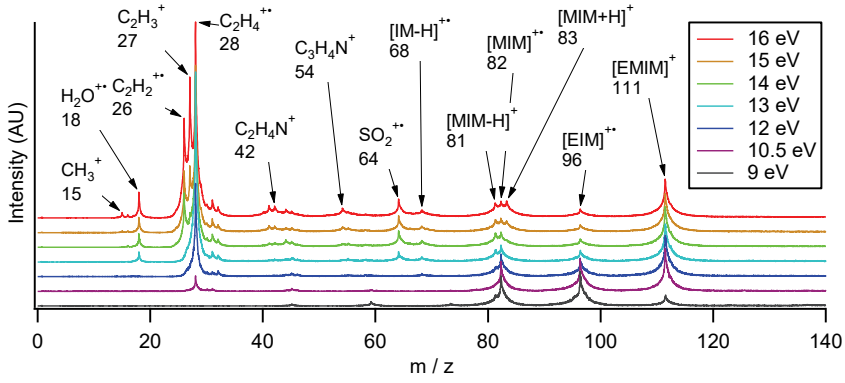

Figure 12. TOF-MS spectra of [EMIM][OTf] measured at different photon energies and acquired at 243 °C. The spectra have been normalized to the m/z 111 peak height and vertically offset, except for the 9 eV curve, which has not been normalized. Excitation photon energies and key fragments are given in the figure. Figure reproduced under a CC BY 4.0 license from (Paper II).

Besides the separation of the anion and cation from the isolated ion pair, three fragmentation channels can be identified. The first one involves the loss of the methyl (-CH_3) group and produces $[EIM]^{+\bullet}$ fragments (m/z 96). The second one involves the loss of the ethyl (-C_2H_5) group and produces $[MIM\text{-}H]^+$, $[MIM]^{+\bullet}$ or $[MIM+H]^+$ fragments. At excitation energies 15 and 16 eV, the corresponding triple peak feature at m/z 81–83 can be clearly observed (Figure 12). The third fragmentation channel involves the loss of both alkyl groups and produces dehydrogenated $[IM\text{-}H]^{+\bullet}$ (m/z 68).

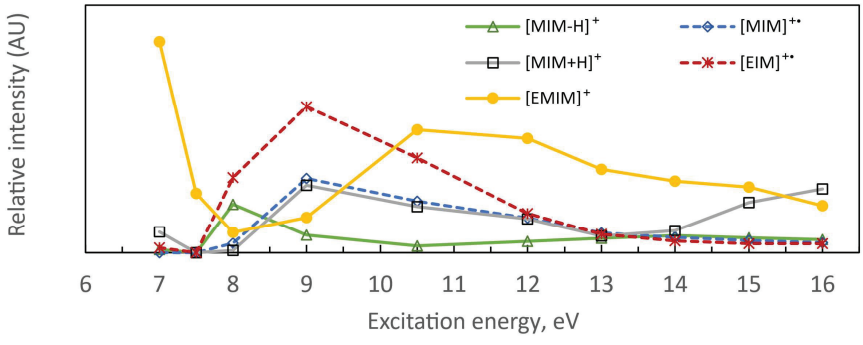

Figure 13. The relative intensity (peak intensity relative to the sum of IL-related fragments) of the main fragments of [EMIM][OTf] as a function of excitation energy. Dotted lines represent odd electron fragments and solid lines even electron fragments. The $[MIM+H]^+$ curve has been multiplied by 4 for better visual comparison. Figure reproduced under a CC BY 4.0 license from (Paper II).

The peak intensity of the main fragments of [EMIM][OTf] varies with energy, as shown in Figure 13. At low energies, the intensity of the main cation peak (m/z 111) is high, then it drops significantly at around 9 eV and then rises again at higher excitation energies. It has been interpreted analogously to our group's previous study of [EMIM][BF_4] in [59]. When the photon energy is below the ionization threshold, but over the first photoexcitation resonance, the IL is photoexcited and can fragment into its cation and anion constituents (according to Equation 3). When the photon energy is raised over the photoexcitation threshold energy, but is still below the ionization energy, the signal decreases because the photo-absorption cross-section decreases. Starting from the photoionization threshold, the cation peak signal starts to increase again. This analysis is based on the assumption that there are many excited states below the ionization threshold, similar to [EMIM][BF_4][59]. These states are dissociative and result in various fragments. An extensive study of excited states of several ILs using electron energy loss spectroscopy (EELS), UPS and DFT [75] further supports this analysis. Unfortunately, the lack of sufficient data points prevents us from determining the ionization energy precisely, but it is approximately 10 eV.

Secondly, the two dominant cation fragmentation peaks $[MIM]^{+\bullet}$ and $[EIM]^{+\bullet}$ seem to behave similarly. Therefore, it is assumed that the fragmentation to $[MIM]^{+\bullet}$ and $[EIM]^{+\bullet}$ are probabilistic outcomes from the same initial state.

Thirdly, the $[MIM]^{+\bullet}$ at m/z 82 and the hydrogenated $[MIM+H]^{+}$ peak at m/z 83 behave almost identically at low energies. From about 14 eV onwards, the $[MIM+H]^{+}$ diverges to higher intensity compared to $[MIM]^{+\bullet}$. Therefore, the fragmentation to $[MIM]^{+\bullet}$ or to $[MIM+H]^{+}$ seems to be competing decay channels, and when more energy is deposited, the system seems to prefer the $[MIM+H]^{+}$ fragmentation channel.

The following conclusion has been drawn from these behaviors: there is no reason to assume the presence of a hydrogenated [EMIM][OTf] in the liquid phase, as the $[MIM]^{+\bullet}$ and $[MIM+H]^{+}$ peaks are naturally explained.

However, the presence of dehydrogenated [EMIM][OTf] cannot be ruled out. A weak signal of the dehydrogenated $[EMIM-H]^{+}$ at m/z 110 was detected already at 110 °C during heating (not shown on any figures). This signal originates from the modification of the IL by the residuals inside the IL, as discussed in reference [76]. The dehydrogenated $[MIM-H]^{+}$ peak at m/z 81 behaves differently from other peaks (Figure 13). Its intensity seems to be anti-correlated to the intensity of the $[EMIM]^{+}$ peak at m/z 111, and therefore, it could result from thermal decomposition products. Furthermore, unlike in the case of [EMIM][BF_4] [59], the dehydrogenated $[EIM-H]^{+\bullet}$ at m/z 95 is not observed in [EMIM][OTf].

5.2.3 [EMIM][DCA]

The TOF-MS spectra of [EMIM][DCA] were acquired at different photon energies at a temperature of 140 °C (see Figure 14).

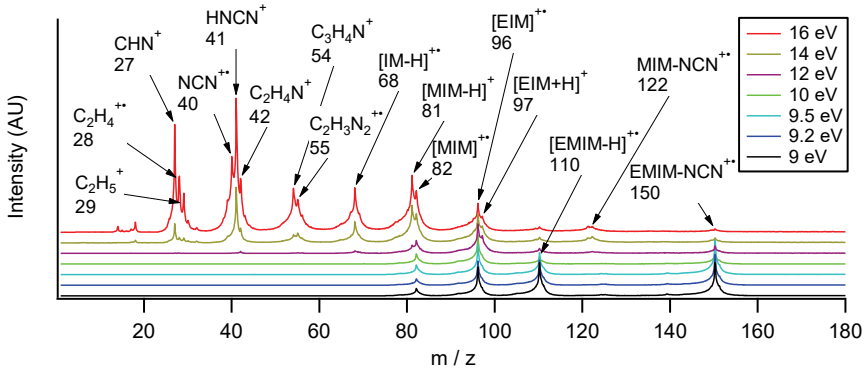

Figure 14. TOF-MS spectra of [EMIM][DCA]. The spectra have been normalized to the m/z 96 peak height and offset vertically. Excitation photon energies and key fragments are given in the figure. Figure reproduced under a CC BY 4.0 license from (Paper II).

The $[EIM]^{+\bullet}$ fragment at m/z 96 and the hydrogenated $[EIM+H]^{+}$ fragment at m/z 97 have very similar energy dependencies. A similar conclusion has been drawn as in the [EMIM][OTf] case from this data: the fragmentation to $[EIM]^{+}$ or to $[EIM+H]^{+}$ seems to be competing decay channels from the same initial state. Again, there is no need to suppose the presence of hydrogenated [EMIM][DCA] but rather the $[EIM+H]^{+}$ peak results from the cleavage of the methyl group when it leaves a hydrogen behind (i.e. a net loss of CH_2).

The peak at m/z 150 is likely a liquid phase reaction product [76, 77], EMIM-$NCN^{+\bullet}$ (NCN-ylidene), involving the carbene intermediate. It is well-known that carbenes are highly reactive [78, 79] and the respective mechanism is proposed by Chambreau *et al.* [76, 77].

It was also suggested in (Paper II) that the reaction product EMIM-NCN is formed in liquid phase and is not a result of gas phase interactions. In our experiment, the experimental chamber pressure increased over time even when the effusion cell temperature was kept constant for 4 hours. In our experience, if the only process involved is thermal evaporation, then the experimental chamber pressure should decrease over time as the water evaporates from the IL and outgassing from the vacuum chamber's inner surface occurs. The constant increase in pressure over time can be caused by thermal decomposition of the IL or chemical reactions inside the IL. As the experiment was carried out at 140 °C, well below the reported 284 °C thermal decomposition temperature of [EMIM][DCA] [80], a plausible explanation is that the decrease of the water content creates an environment where chemical reactions can take place to produce EMIM-$NCN^{+\bullet}$. Chambreau et al. even proposed that this could be a useful one-pot synthesis

method for NCN imidazolium-ylide species without the need for flammable solvents at lower temperatures than reported previously [76].

The peak at m/z 122 is the fragments resulting from the loss of an ethyl group from the EMIM-$NCN^{+\bullet}$ reaction product. This assignment is based on the fact that the fragment has a m/z 28 difference from the EMIM-$NCN^{+\bullet}$ parent compound, which indicates a loss of an ethyl group when it leaves hydrogen behind. As with $[EMIM]^+$ fragments involving alkyl group losses, the dehydrogenated species MIM-NCN-$H^{+\bullet\bullet}$ can also be observed at m/z 121. The peak at m/z 110 is assigned to dehydrogenated $[EMIM\text{-}H]^{+\bullet}$.

5.2.4 Comparison of ionic liquids

In the case of all investigated ILs [EMMIM][TFSI], [EMIM][OTf] and [EMIM][DCA], the intact cation peaks were identified and the cation fragments were observed. No higher mass positively charged clusters were detected in any case. This indirectly confirms that ILs vaporize as isolated ion pairs.

Deyko *et al*. concluded that the intact cation to main fragment ratio (relative yield) seems to depend on the anion size [36]. Therefore, the area of the intact cation peak to the sum of the areas of the main cation fragments were compared (e.g. sum of $[MIM]^{+\bullet}$, $[MMIM]^+$ and $[EIM]^{+\bullet}$ in case of [EMMIM][TFSI]). Such ratio was highest (86 at 10.5 eV ionization energy) for [EMMIM][TFSI] and lowest (12 at 9 eV ionization energy) for [EMIM][DCA] (Paper II). Tolstogouzov *et al*. performed a TOF-MS experiment on [EMIM][TFSI] using 20 eV electron ionization and observed a fragment-to-parent cation ratio that seems to be roughy similar to our results of [EMMIM][TFSI] [81]. However, a 70 eV electrospray ionization line-of-sight MS experiment of [EMIM][TFSI] demonstrated a lower ratio [36]. Our experiment seems to partially support Deyko *et al-s* hypothesis that ILs with larger anions have fewer cation fragments. It has to be noted that, in addition to anion size, cation fragmentation ratio is also dependent on the anion species, ionization method, and ionization energy.

TOF-SIMS spectra of [EMIM][TFSI] have been reported previously [82–84]. Both 2 keV He^+ and 2.5 keV Ga^+ were used for excitation. The cation fragment peak assignment of these works looks remarkably similar to our [EMIM][OTf] TOF-MS spectra with 16 eV excitation energy. The cation fragment peaks have less intensity in the TOF-SIMS study of [EMIM][TFSI] [73] when compared to our [EMIM][OTf] results (Figure 12), but the main fragment peaks $[MIM]^{+\bullet}$, $[MIM+H]^+$ and $[EIM]^{+\bullet}$ in our case seem to be in roughly the same proportion with respect to each other like in work by Souda et al. [83]. If to compare the TOF spectra of [EMIM][TFSI] [83] with the TOF spectra of [EMIM][OTf] (Figure 12), the main difference is the higher intensity of peaks at m/z 40–42 and 52–56 in our work. The peaks in these regions are associated with the fragmentation of the imidazolium ring. The ring cleavage is more probable with higher excitation energies [85, 86].

Even at low temperatures of 140 °C, the temperature-induced reaction product 2-cyanoimino-1-ethyl-3-methylimidazole EMIM-$NCN^{+\bullet}$ at m/z 150 was observed

in the TOF-MS spectra of [EMIM][DCA]. The additional peaks originating from EMIM-$NCN^{+\bullet}$ in the TOF-MS spectra of [EMIM][DCA] make it difficult to compare [EMIM][DCA] (Figure 14) and [EMIM][OTf] (Figure 12) spectra directly. Both $[EMIM]^+$ based ILs produce preferably $[EIM]^{+\bullet}$ fragments at lower (below 12 eV) excitation energies. In addition, [EMIM][OTf] spectrum exhibits a triple peak feature for $[MIM\text{-}H]^+$, $[MIM]^{+\bullet}$ and $[MIM+H]^+$. The $[EMIM]^+$ cation and the hydrogenated $[MIM+H]^+$ are not present in the [EMIM][DCA] spectrum, but the hydrogenated $[EIM+H]^+$ and dehydrogenated $[EMIM\text{-}H]^+$ fragments are observed. [EMMIM][TFSI] (Figure 11), however, produces different fragments than $[EMIM]^+$ based ILs: $[MMIM\text{-}H]^+$ and $[MMIM]^+$ peaks are observed, and no hydrogenated species are detected.

[EMIM][OTf] exhibits a triple peak feature consisting of $[MIM\text{-}H]^+$, $[MIM]^+$ and $[MIM+H]^+$. The $[MIM]^+$ and $[MIM+H]^+$ fragments of [EMIM][OTf] were seen to behave very similarly with respect to excitation energy. This is also the case for $[EIM]^+$ and $[EIM+H]^+$ fragments in [EMIM][DCA]. It was concluded that in each case, they result from the same initial state, and there is no need to assume the presence of hydrogenated [EMIM][DCA] or [EMIM][OTf] species in the liquid phase.

In the case of [EMMIM][TFSI] the loss of a methyl group from the nitrogen position should produce a $[EMIM]^+$ peak at m/z 111. However, in [EMMIM] [TFSI] this peak was not observed in the photon energy range of 10.5 to 16 eV. [EMMIM][TFSI] produces different fragments than $[EMIM]^+$ based ILs: $[MMIM\text{-}H]^+$ and $[MMIM]^+$ are observed and no hydrogenated species are detected.

5.3 Paper III – The electronic structure of ionic liquids based on the TFSI anion: A gas phase UPS and DFT study

This is the first-ever research paper published based on experiments conducted at the FinEstBeAMS beamline. In this paper, the valence bands of [EMIM][TFSI], [DEME][TFSI] and $[PYR_{14}][TFSI]$ gas-phase ion pairs have been investigated using UPS. To the best of our knowledge, this is the first presentation of the vapor phase UPS spectra of two [TFSI] based ionic liquids: [DEME][TFSI] and $[PYR_{14}][TFSI]$.

[EMIM][TFSI] (purity ≥98%), $[PYR_{14}][TFSI]$ (purity ≥98.0%) and [DEME] [TFSI] (purity ≥98.5%) were purchased from Sigma Aldrich. Gas-phase experiments were carried out by evaporating the liquid from a quartz crucible of an effusion cell. After inserting 5 ml of IL into the effusion cell (NTEZ, MBE Komponenten, Germany), heating of IL at 80 °C for several hours was performed to remove residual water from the ILs. The ILs themselves were evaporated at 220–240 °C.

The main experimental result of this paper is that all three investigated ionic liquid vapors demonstrate similar photoelectron spectra because all three ILs have the $[TFSI]^-$ anion (Figure 16, upper part). UPS spectra were measured with an excitation energy of 40 eV for the ionic liquids [EMIM and $PYR_{14}][TFSI]$ and

50 eV for [DEME][TFSI]. The similar shapes of the experimental spectra suggested that all three UPS spectra are primarily influenced by the TFSI anion. This conclusion was fully supported by *ab initio* calculations.

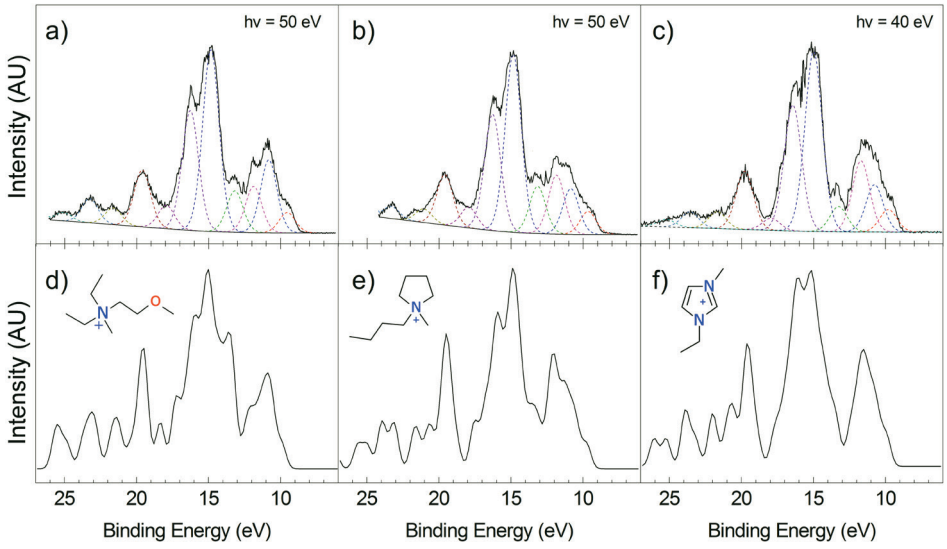

Figure 15. Side-by-side comparison of experimental and calculated spectra with the depiction of the cation as inset. a) and d) [DEME][TFSI], b) and e) [PYR_{14}][TFSI], c) and f) [EMIM][TFSI]. All simulated density of states (DOS) type spectra have been calculated using the hybrid ωB97X-D functional. The dotted curves that are fitted on a), b), c) experimental spectra are for eye-guide only. Figure modified under a CC BY 4.0 license from (Paper III).

The experimental photoelectron spectra are interpreted by using several density functional and *ab initio* calculation methods. However, when discussing intensities, it is important to remember that the intensity of photoemission does not depend on the density of states only [35] but also on the experimental geometry, electron analyzer transmission function, incident photon energy and photoemission cross sections among other parameters. The good accordance of experimental UPS spectra (Figure 15, upper part) and *ab initio* DOS calculation (Figure 15, lower part) also indirectly confirms that isolated IL molecules dominate in the vapor phase.

Calculations demonstrate that the HOMO state (lower binding energy side of UPS spectra) of the [DEME][TFSI] ion-pair is due to the $[TFSI]^-$ anion, while in [EMIM][TFSI] it is due to the $[EMIM]^+$ cation. However, it is difficult to make conclusive assignments for the [PYR_{14}][TFSI] ionic liquid. All calculation methods predict the LUMO to be of cationic origin in all the studied ion pairs.

It is also important to point out that the HOMO-LUMO gaps predicted by the hybrid M06 functional are reversed when compared to the experimental electrochemical stabilities. For example, the IL whose ion pairs have the largest calculated HOMO-LUMO gap ([EMIM][TFSI]) is actually electrochemically the least

stable. This seems to verify the claim that the HOMO-LUMO gaps from the calculation should not be blindly used to make conclusions about the anodic or cathodic stabilities.

5.4 Paper IV – Ionic Liquid Vapors in Vacuum: Possibility to Derive Anodic Stabilities from DFT and UPS

In (Paper III), it was confirmed that UPS spectroscopy can be successfully applied to vapor-phase ILs. In (Paper IV), the scope was widened, and more ILs were included. It was determined that the M06 functional was able to reproduce most of the spectral features, and it performed surprisingly well for most IL vapors.

UPS measurements were conducted in a pressure range of 10^{-7} mbar using a liquid nitrogen-cooled cold trap. Due to the high hydrophilicity of some ionic liquids (ILs) and their significant water content, water continued to evaporate even at elevated temperatures. As a result, traces of water vapor are present in most spectra, specifically contributing peaks at 12.62 eV and 13.0 eV. Additionally, because of the relatively low vapor density of the ionic liquid, various background gases are also detected in the spectra, with nitrogen being the most prominent. Nitrogen contributes peaks at 15.6 eV, 16.7 eV, 16.9 eV, 17.15 eV, and 18.75 eV. In most instances, the peaks from background gases do not significantly affect the interpretation of the spectra.

Knowledge of the electronic energies and composition of the topmost valence states (HOMO region) is vital for understanding processes that involve the removal of electrons from the IL [87]. Due to the high practical importance of the EW and the very large number of *ab initio* calculation studies of ionic liquid ion pairs in vacuum, further experimental data on the HOMO (and LUMO) states of ionic liquid ion pairs are needed. In the future, LUMO states could be investigated further using Inverse Photoemission Spectroscopy (IPS).

UPS investigations of several gas-phase IL ion pairs have been conducted. The criteria for selecting the following ILs are outlined in Section 4.1. [EMIM][OTf], [PYR_{14}][OTf], [EMIM][DCA], [PYR_{14}][DCA], [PYR_{14}][TCM], [PYR_{14}][FSI], [PYR_{14}][PF_6], [S_{222}][TFSI], [P_{4441}][TFSI], and [EMMIM][TFSI] vapor UPS spectra are presented for the first time at the time of the release of this paper. DFT calculations have been used to interpret the experimental data. The gas-phase photoelectron spectra in conjunction with the theoretical calculations are able to verify most HOMO energies and assign them to the cation or anion.

Many different ion-pair conformers were manually constructed. All geometries (conformers) were optimized (relaxed) for the lowest energy. For example, over 40 different conformers were studied for [S_{222}][TFSI]. Similarly to Fogarty et al., the emphasis was to survey a wide range of cation–anion placements [88].

The measured ILs with the $[TFSI]^-$ anion [EMMIM][TFSI], [P_{4441}][TFSI], and [S_{222}][TFSI] (Paper IV) have similar UPS spectra. Their spectra are also similar

to the UPS spectra of other $[TFSI]^-$ anion-based ILs like $[PYR_{14}][TFSI]$, [DEME][TFSI] (Paper III), [EMIM][TFSI] [89], [BMIM][TFSI] [90], etc. This is because their spectra are mostly dominated by the anion. However, the low-energy region around 9–12 eV is still somewhat different in all of the $[TFSI]^-$ anion-based ILs. As mentioned above, the low-binding-energy cutoff value of the $[TFSI]^-$ anion-based IL vapors is about 8.6–8.7 eV. The $[TFSI]^-$ anion-based ILs are also the most thermally stable under our experimental setup, i.e., they can be evaporated in high vacuum with minor thermal degradation. The UPS data shows that in general, the HOMO energies of IL ion pairs are increasing with increasing electron affinity of the anion: $[DCA]^-$, $[OTf]^-$, $[TFSI]^-$, $[FSI]^-$, $[BF_4]^-$, $[PF_6]^-$. Therefore, we predict that the $[TFSI]^-$ anion should be more stable than the $[OTf]^-$ anion. This is in agreement with results of Asha et al [91, 92].

The DFT calculation predicts that the HOMO of presented $[DCA]^-$ and $[TCM]^-$ anion-based ILs is due to the π-orbitals of the anion. Furthermore, the top six molecular orbitals of $[PYR_{14}][DCA]$ and $[PYR_{14}][TCM]$ are associated with the π-orbitals of the anion.

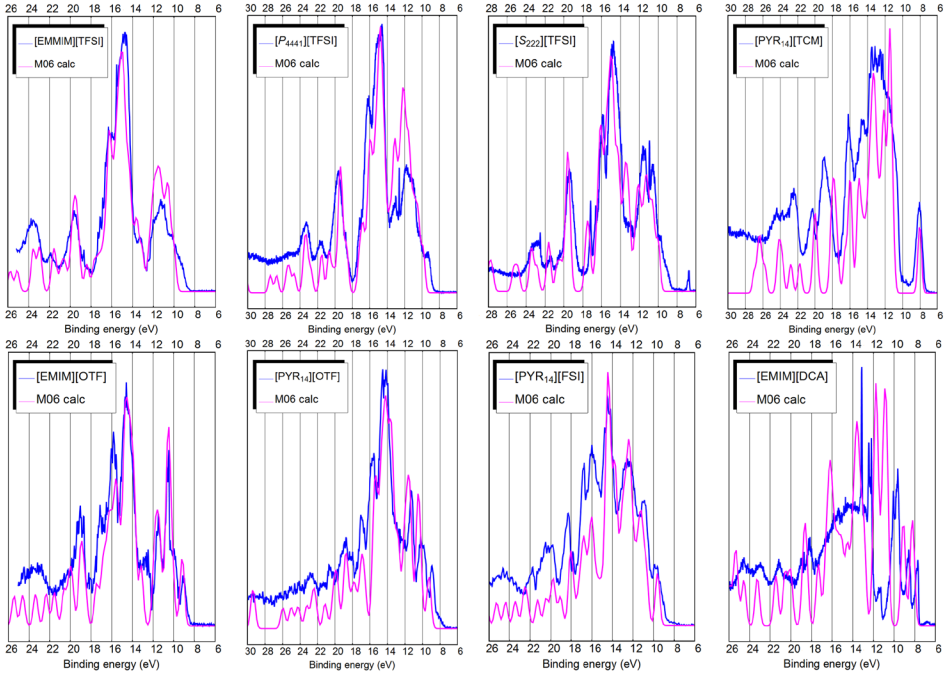

Figure 16. Experimental UPS spectra (blue curves), and DFT DOS simulations (magenta curve) of IL ion pairs. Figure modified under a CC BY 4.0 license from (Paper IV).

In some cases ($[PYR_{14}][FSI]$, $[PYR_{14}][TCM]$), the excellent agreement between the experimental UPS spectrum and the calculated DOS (Figure 16) validates the conformer found for the IL ion pair and provides indirect experimental evidence for the structure of ionic liquid vapors. This is due to the sensitivity of the UPS spectrum on the underlying ion-pair structure.

The acquired experimental data together with new insights on the charge transfer process enabled the reinterpretation of the HOMO energy of [EMIM][BF_4]. The binding energy of the HOMO of [EMIM][BF_4] ion pair was estimated to be 9.25–9.3 eV instead of the previous estimation of 7.4 eV. This is suggested by the overall agreement with our calculation trends.

At the time of publication (Paper IV) only a limited number (10+) of experimental photoelectron spectra of IL vapors were available in the literature. However, the liquid phase IL energy gaps of imidazolium-based ionic liquids determined by Kanai et al. [33] with UPS/IPS methods are in excellent agreement with our gas-phase HOMO data and the M06 (calculation is shifted by +1 eV) calculations. Using UPS and IPS, Kanai et al. [33] showed that [OMIM][BF_4] has a HOMO-LUMO gap of 9.1 eV. That IL is expected to have a very similar gap to [EMIM][BF_4] and [BMIM][BF_4]. Indeed, the UPS/IPS method is a direct probe of the valence and conduction bands. Therefore, this method is recommended for future IL studies.

5.5 Paper V – Charge transfer and electronic relaxation effects in the photoemission of EMIM-DCA ionic liquid vapor

The difficulties in calculating the electronic structure of ILs have been pointed out many times already [9, 93–95] (Paper III–IV). From the wide selection of ILs, investigated in the present thesis, the hybrid M06 DFT functional only had difficulties with the description of the electronic structure of [EMIM][DCA] (as shown in (Paper IV). This contrasts with many other ILs where the hybrid M06 functional performed remarkably well [96] (Paper III–IV). Therefore, further analysis of the [EMIM][DCA] electronic structure has been done in Paper V.

Our calculations show that the [EMIM][DCA] electronic structure is highly sensitive to the underlying ion-pair structure. Our previous work with the electronic structure of various ILs also revealed a strong dependence on the calculation method (Paper III–IV), [96, 97].

Figure 17 demonstrates the predicted conformer structure of the [EMIM][DCA] ion-pair (left) and the proposed charge transfer state (right). The $[DCA]^-$ anion is very simple compared to most ILs anions and the [EMIM][DCA] itself only has hydrogen, carbon and nitrogen atoms present. We have chosen the conformer, whose DOS type spectra offers the best overall agreement with the experimental UPS spectrum.

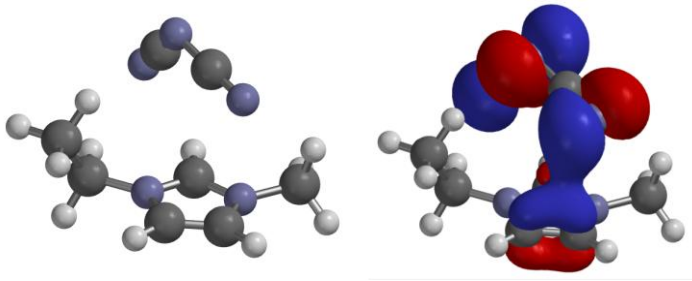

Figure 17. The predicted conformer structure of the ion-pair(left) and the proposed charge transfer state (right). Hydrogen atoms are marked with light grey, carbon atoms with dark grey and nitrogen atoms with dark purple. The blue and red areas indicate the electron density associated with positive and negative phases. Figure reproduced under a CC BY 4.0 license from (Paper IV).

The charge distribution analysis based on the MP2 wavefunction of the ion-pair shows that the neutral [EMIM][DCA] ion-pair has a cation-anion charge of ±0.76e. However, from the calculations follows that the ionized molecule (ionized ion-pair) has cation-anion charges of +2.15e and –1.15e. Therefore, in addition to the removal of an electronic charge upon ionization, this suggests a possible further charge transfer of about –0.39e from the cation to the anion. This is the explanation behind the charge transfer/electronic relaxation effect indirectly observed in the UPS spectrum. The electronic relaxation process during photoemission was already found in [EMIM][BF_4][96]. However, in [EMIM][BF_4], the relaxing states seem to be reversed compared with the [EMIM][DCA] studied in this thesis. In that IL, the cation-related peaks seemed to relax, while the $[BF_4]^-$ anion remained mostly intact [96].

Our preliminary analysis shows that a π–π* type transition occurs during the photoemission of both ILs. In [EMIM][BF_4], this transition is on the $[EMIM]^+$ cation itself, and in [EMIM][DCA], it is interionic: from the cation to the anion. Such charge transfer during photoemission is rare, uncommon, and needs more theoretical and experimental research.

Therefore, the charge distribution differences between ionized [EMIM][BF_4] and [EMIM][DCA] ion pairs can explain differences in their UPS spectra, especially the relaxation behavior. Furthermore, the difference in the electronic relaxation between [EMIM][BF_4] and [EMIM][DCA] must be due to the anion, since the cation is the same.

Recently, in unpublished results, the band gap of [EMIM][BF4] has been even more accurately re-evaluated to be 9.85 eV.

The conclusion of (Paper V) is that along with [EMIM][BF_4] and [EMIM][$B(CN)_4$][98] also [EMIM][DCA] provides another example of the need for further improvements in DFT based calculations to match the qualitative accuracy of wavefunction based *ab initio* calculation methods.

6. CONCLUSIONS

This thesis is dedicated to investigations of the electronic structure of selected ILs in the vapor phase. In this research, the effects of different anion and cation combinations on the electronic structure of ionic liquids were studied. These results were compared with *ab initio* electronic structure calculations (MP2, DFT) of the same compounds to offer high quality experimental data and to give feedback for theoretical calculations.

All experiments of the present thesis were performed at the new FinEstBeAMS beamline at the MAX IV Laboratory (Lund, Sweden). The author designed and implemented an effusion cell-based experimental apparatus that enabled the vaporization of ILs and their vapor phase photoelectron spectroscopy measurements and mass spectrometry measurements.

The building and commissioning of the FinEstBeAMS beamline was a 7-year-long group effort in which the author of the present thesis contributed. The author participated in the assembly, optimization and characterization of the FinEstBeAMS beamline and preparation of the solid-state branch including endstation for commissioning. The beamline was put into operation, and it was confirmed that the performance of the beamline was as designed (Paper I). It is noteworthy that the achieved resolution of the beamline was even better than initially planned.

The first-ever UPS spectra of more than 10 ionic liquid vapors were measured and interpreted: [EMMIM][TFSI], [EMIM][OTf], [EMIM][DCA], [EMIM][TFSI], $[PYR_{14}][TFSI]$, $[PYR_{14}][OTf]$, $[PYR_{14}][DCA]$, $[PYR_{14}][TCM]$, $[PYR_{14}][FSI]$, $[PYR_{14}][PF_6]$, $[S_{222}][TFSI]$, $[P_{4441}][TFSI]$, [DEME][TFSI] (Paper III–V). The first TOF-MS spectra of [EMMIM][TFSI] and [EMIM][OTf] were reported (Paper II). Our selection of ILs was diverse, and it included simple sulfonium-based, ammonium-based, phosphonium-based, imidazolium-based aromatic cations, non-aromatic rings like pyrrolidinium $[PYR_{14}]^+$; and small anions such as $[PF_6]^-$, medium-sized anions like $[FSI]^-$, $[OTf]^-$ and large anions like $[TFSI]^-$.

It has been shown that it is possible to experimentally determine the electronic structure (Paper III–V) and fragmentation patterns of IL vapors (Paper II). This is not trivial, since several experimental parameters and requirements for the IL have to be considered. Firstly, high photon flux is needed for vapor phase UPS experiments due to the very low vapor pressure of most ILs. Secondly, not every IL is suitable for vapor phase experiments in a vacuum – in some cases thermal degradation takes place even below evaporation temperature.

TOF-MS detected intact IL cations, and no positively charged clusters with higher mass than the cation were observed (Paper II). This also indirectly confirmed that ILs vaporize as isolated ion pairs. TOF-MS results revealed that ILs with larger anions have less cation fragmentation. Also, the breakup of the ring is more probable with excitation energy higher than 12 eV. The presence of hydrogenated and dehydrogenated cation fragments (Paper II) was confirmed in [EMMIM][TFSI], [EMIM][OTf] and [EMIM][DCA]. It was found in the case of [EMIM][OTf] and [EMIM][DCA] that there is also a different ratio of hydrogenated and dehydrogenated $[EMIM]^+$ fragments. The dissociation mechanisms

underlying the hydrogenation and dehydrogenation of the cation fragments require further clarification.

The presence of isolated IL molecules in the vapor phase was confirmed by the good agreement between the UPS spectra and the *ab initio* calculations for most of the studied ILs (Paper III–V), because all the DFT calculations used isolated ion pairs as the underlying structure. The UPS spectra of $[PYR_{14}][FSI]$ and $[PYR_{14}][TCM]$ showed especially good agreement with theory (Paper IV).

The UPS experimental data show that the HOMO energies of ILs increase with the electron affinity of the anion in ascending order: $[DCA]^-$, $[OTf]^-$, $[TFSI]^-$, $[FSI]^-$, $[BF_4]^-$, $[PF_6]^-$. In general, a more negative HOMO energy implies greater stability. There are conflicting reports on the relative stability of $[TFSI]^-$ and $[OTf]^-$ in the literature. Based on our data, it can be estimated that the $[TFSI]^-$ anion is more stable than the $[OTf]^-$ anion (Paper IV).

Modern quantum chemistry calculations (hybrid DFT, GW, MP2) can describe most UPS spectra (Paper III–V). In some cases ($[PYR_{14}][FSI]$ and ($[PYR_{14}][TCM]$), the excellent agreement between the experimental UPS spectrum and the calculated DOS validates the conformer found for the IL ion-pair and provides indirect experimental evidence for the structure of ionic liquid vapors. This is possible due to the sensitivity of the UPS spectrum on the underlying ion-pair structure (Paper IV). To clarify, this is not always the case: if different conformers do not produce considerable changes in the calculated DOS-type spectra, then it is difficult to determine which conformers were present in the experiment.

The acquired experimental data, together with previous experimental data about other ILs, enabled the reinterpretation of the HOMO energy of $[EMIM][BF_4]$. The binding energy of the HOMO of $[EMIM][BF_4]$ ion pair was estimated to be 9.25–9.3 eV instead of the previous estimation of 7.4 eV (Paper IV). More recent calculations (unpublished results from 2025), reinterpret the HOMO energy of $[EMIM][BF_4]$ to be even higher at 9.85 eV.

However, there are exceptions to the good agreement between theory and experiment, and this was the case for [EMIM][DCA] in (Paper IV). These discrepancies were resolved, and the key reason was found to be a rare and uncommon charge-transfer process. Indeed, it has been shown that in the case of [EMIM][DCA], there are strong indications that electronic relaxation during photoemission is occurring (Paper V). Furthermore, the charge distribution differences between ionized $[EMIM][BF_4]$ and [EMIM][DCA] ion pairs were used to explain the differences in their UPS spectra, especially in their relaxation behavior.

This thesis has advanced the understanding of ILs' electronic structure in the vapor phase through high quality UPS and TOF-MS measurements at the FinEstBeAMS beamline. The results confirmed the existence of isolated ion pairs in vapor phase, which is in agreement with *ab initio* calculations. Key findings include the influence of anion electron affinity on HOMO energies and the identification of charge-transfer processes in specific ILs, such as [EMIM][DCA]. The findings reported herein help clarify existing ambiguities in the literature, provide quality data and analysis for future electronic structure investigations of IL in the vapor and in the liquid phase.

SUMMARY IN ESTONIAN

Fotoergastatud protsessid ioonvedelike aurudes

Käesolev doktoritöö on pühendatud valitud ioonvedelike elektronstruktuuri uurimisele aurufaasis. Täpsemalt uuriti erinevate anioonide ja katioonide kombinatsioonide mõju ioonsete vedelike elektronstruktuurile. Saadud tulemusi võrreldi samade ühendite *ab initio* elektronstruktuuri arvutustega (MP2, DFT), et pakkuda kvaliteetseid katseandmeid ja anda tagasisidet teoreetiliste arvutuste täpsustamiseks.

Kõik käesoleva dissertatsiooni eksperimendid viidi läbi MAX IV labori FinEstBeAMS kiirekanalil. Autor disainis ja rakendas efusioonrakul põhineva eksperimentaalse lahenduse, mis võimaldas ioonsete vedelike aurustamist, nende aurufaasi fotoelektronspektrite ning massispektrite mõõtmist.

FinEstBeAMS kiirekanali ehitamine ja kasutuselevõtt oli 7 aastat kestnud grupitöö, milles ka käesoleva dissertatsiooni autor osales. Autor osales FinEstBeAMS kiirekanali monteerimisel, optimeerimisel ja karakteriseerimisel ning kiirekanali tahkise haru lõppjaama ettevalmistamises kasutuselevõtuks. Kiirekanal rakendati tööle ning näidati ära, et kiirekanali parameetrid reaalsetes töötingimustes vastasid põhiosas algselt kavandatule (Artikkel I). On märkimisväärne, et kiirekanalil saavutatud spektraallahutus oli parem kui algselt planeeritud.

Esmakordselt mõõdeti ja interpreteeriti üle kümne aurufaasis oleva ioonvedeliku fotoelektronspektrid: [EMMIM][TFSI], [EMIM][OTf], [EMIM][DCA], [EMIM][TFSI], [PYR_{14}][TFSI], [PYR_{14}][OTf], [PYR_{14}][DCA], [PYR_{14}][TCM], [PYR_{14}][FSI], [PYR_{14}][PF_6], [S_{222}][TFSI], [P_{4441}][TFSI], [DEME][TFSI] (Artiklid III–V). Esmakordselt registreeriti ja analüüsiti [P_{4441}][TFSI] ja [DEME][TFSI] lennuaja-massispektrid (TOF-MS) (Artikkel II). Uuringuteks valiti lihtsamad sulfooniumi- $[S_{222}]^+$, ammooniumi- $[DEME]^+$, fosfooniumipõhised $[P_{4441}]^+$ katioonid, aromaatsed katioonid nagu $[EMIM]^+$, mittearomaatse rõngaga katioon $[PYR_{14}]^+$. Valiti väikesed anioonid $[PF_6]^-$, keskmise suurusega anioonid $[FSI]^-$, $[OTf]^-$ ning suured anioonid $[TFSI]^-$.

Näidati, et gaasfaasis ioonvedelike elektronstruktuuri [Artiklid III–V] ja massispektreid (Artikkel II) saab eksperimentaalselt määrata. See pole triviaalne, kuna tuleb silmas pidada mitmeid eksperimentaalseid parameetreid ja nõudeid ioonvedelikele. Esiteks, aurufaasi ultraviolett fotoelektronspektroskoopia (UPS) eksperimentide jaoks on vaja suurt footonite voogu, kuna ioonvedelikel on väga madal aururõhk. Teiseks, mitte kõik ioonvedelikud ei sobi aurufaasi eksperimentideks – osadel juhtudel toimub termiline lagunemine enne aurustustemperatuurini jõudmist.

TOF-MS mõõtmiste käigus tuvastati terveid IL katioone ja katioonist suurema massiga laetud klastreid ei leitud (Artikkel II). See tõestab kaudselt, et ioonvedelikud aurustuvad isoleeritud ioonpaaridena. TOF-MS tulemused näitasid, et suuremad katioonid fragmenteeruvad vähem ja aromaatse ringi purunemise tõenäosus suureneb ergastusenergiatel üle 12 eV. Hüdrogeneerunud ja dehüdrogeneerunud fragmentide olemasolu tehti kindlaks [EMIM][OTf], [EMIM][DCA] ja [EMMIM][TFSI] puhul. Leiti, et [EMIM][OTf] ja [EMIM][DCA] puhul on

hüdrogeneerunud ja dehüdrogeneerunud $[EMIM]^+$ fragmentide osakaal erinev (Artikkel II). Eriti need dissosatsiooni mehhanismid, mis puudutavad seesuguseid hüdrogeneeritud ja dehüdrogeneeritud fragmente, vajavad siiski edasist uurimist.

Isoleeritud IL molekulide (ioonpaaride) olemasolu aurufaasis tehti kindlaks UPS spektrite ja *ab initio* arvutuste hea kooskõlaga enamuse ioonsete vedelike puhul (Artiklid III–V). Kõikide DFT arvutuste puhul kasutati põhistruktuuriks isoleeritud ioonpaare, seejuures $[PYR_{14}][FSI]$ ja $[PYR_{14}][TCM]$ UPS spektrid olid eriti heas kooskõlas teooriaga (Artikkel IV).

Meie gaasifaasi UPS andmete põhjal saame teha järelduse, et üldiselt suurenevad HOMO energiad aniooni elektronegatiivsuse kasvades reas: $[DCA]^-$, $[OTf]^-$, $[TFSI]^-$, $[FSI]^-$, $[BF_4]^-$, $[PF_6]^-$. Negatiivsem HOMO energia viitab suuremale stabiilsusele. Kirjandusest on leida vastuolulisi andmeid $[TFSI]^-$ and $[OTf]^-$ asukohtade suhtes stabiilsusjärjestuses. Lähtudes meie katseandmetest järeldasime, et $[TFSI]^-$ anioonid on stabiilsemad kui $[OTf]^-$ anioonid (Artikkel IV).

Kaasaegsed kvantkeemia arvutused (hübriid DFT, GW, MP2) on võimelised kirjeldama enamikku ioonsete vedelike spektreid (Artiklid III–V). Mõnel juhul ($[PYR_{14}][FSI]$, $[PYR_{14}][TCM]$) kinnitab suurepärane kooskõla eksperimentaalse UPS-spektri ja DOS-tüüpi arvutuse vahel ioonpaaride jaoks leitud konformeeride olemasolu ja annab kaudseid eksperimentaalseid tõendeid ioonvedeliku gaasfaasi struktuuri kohta. Selle põhjuseks on UPS-spektri tundlikkus ioonpaari põhistruktuuri suhtes. Selgituseks, see pole alati nii: kui väiksed geomeetrilised muutused põhistruktuuris ei põhjusta märkimisväärseid muutusi arvututatud DOS-tüüpi spektris, siis ei pruugi olla võimalik kindlaks teha, milline konformeer oli eksperimendis vaatluse all.

Kogutud eksperimentaalandmed koos uute teadmistega laenguülekande protsessist võimaldasid uuesti hinnata $[EMIM][BF_4]$ HOMO energia. Uus hinnang $[EMIM][BF_4]$ HOMO seoseenergiale on 9.25–9.3 eV (Artikkel IV), mis on oluliselt suurem varasemast hinnangust 7.4 eV. Veelgi uuemate arvutuste järgi (avaldamata tulemused aastast 2025) on $[EMIM][BF_4]$ HOMO energia veel kõrgem, 9.85 eV.

Siiski on erandeid teooria ja eksperimendi kooskõlas, nagu see oli [EMIM][DCA] puhul (Artikkel IV). See vastuolu lahendati ja põhjus oli haruldane ja harvaesinev laenguülekande protsess. On näidatud, et [EMIM][DCA] puhul toimub fotoemissiooni ajal laenguülekanne (Artikkel V). Lisaks, ioniseeritud [EMIM][BF4] ja [EMIM][DCA] ioonpaaride laengujaotuse erinevus selgitas ka nende UPS spektrite erinevuse, eriti nende relakseerumise protsessis.

Käesoleva töö tulemusel on suurenenud arusaam ioonvedelike elektronstruktuurist aurufaasis läbi kõrge kvaliteediga UPS- ja TOF-MS-mõõtmiste FinEstBeAMS kiirekanalil. Tulemused kinnitavad isoleeritud ioonpaaride olemasolu aurufaasis, mis on kooskõlas *ab initio* arvutustega. Peamised tulemused hõlmavad aniooni elektronafiinsuse mõju HOMO energiatele ja laengu ülekande protsesside tuvastamist konkreetsetes ioonvedelikes nagu näiteks [EMIM][DCA]. Töös saadud tulemused aitavad kaasa olemasolevate erisuste lahendamisele kirjanduses, pakuvad kvaliteetseid eksperimentaalandmeid ja analüüsi tulevikus läbiviidavatele ioonvedelike gaasfaasi ja vedelfaasi uuringutele.

ACKNOWLEDGEMENTS

I am very grateful to my supervisors Vambola Kisand, Rainer Pärna and to my colleague Ivar Kuusik. Vambola Kisand put in enormous effort for the dissertation and also provided guidance and support. Rainer Pärna helped especially in the start of the doctorate project at MAX IV. Ivar Kuusik's theoretical calculations are a critical component in the project. A heartfelt Thank You goes to the late Prof. Ergo Nõmmiste.

I sincerely thank Juhan Matthias Kahk, Marta Berholts, Arvo Kikas, Arvo Tõnisoo and Tanel Käämbre.

I thank all my family and friends for the support they have given me.

This work was financially supported by the following agencies and foundations: Estonian Research Council (Grants IUT2-25, EAG20, PRG1496), ERF project Graduate School of functional materials and technologies, European Social Fund's Doctoral Studies and Internationalisation Programme DoRa, Estonian Centre of Excellence in Research Projects "Advanced materials and high-technology devices for sustainable energetics, sensorics and nanoelectronics (TK141)" and "Center of Excellence in Sustainable Green Hydrogen and Energy Technologies (TK210).

REFERENCES

1. Dupont, J., *From Molten Salts to Ionic Liquids: A "Nano" Journey.* Accounts of Chemical Research, 2011. **44**(11): p. 1223–1231.
2. Hayes, R., G.G. Warr, and R. Atkin, *Structure and Nanostructure in Ionic Liquids.* Chemical Reviews, 2015. **115**(13): p. 6357–6426.
3. Earle, M.J., et al., *The distillation and volatility of ionic liquids.* Nature, 2006. **439**(7078): p. 831–834.
4. Kaur, G., H. Kumar, and M. Singla, *Diverse applications of ionic liquids: A comprehensive review.* Journal of Molecular Liquids, 2022. **351**.
5. Derecskei, B. and A. Derecskei-Kovacs, *Molecular modelling simulations to predict density and solubility parameters of ionic liquids.* Molecular Simulation, 2008. **34**(10–15): p. 1167–1175.
6. Zhuang, W. and W. Zhu, *Potential risk assessment of ionic liquids based on molecular dynamics simulation.* Soft Computing, 2023.
7. Bedrov, D., et al., *Molecular Dynamics Simulations of Ionic Liquids and Electrolytes Using Polarizable Force Fields.* Chemical Reviews, 2019. **119**(13): p. 7940–7995.
8. Cooper, R., et al., *IR and UV Spectroscopy of Vapor-Phase Jet-Cooled Ionic Liquid emim (+) Tf2N (–): Ion Pair Structure and Photodissociation Dynamics.* Journal of Physical Chemistry A, 2013. **117**(47): p. 12419–12428.
9. Strasser, D., et al., *Photoelectron spectrum of isolated ion-pairs in ionic liquid vapor.* J Phys Chem A, 2007. **111**(17): p. 3191–5.
10. Strasser, D., et al., *Tunable wavelength soft photoionization of ionic liquid vapors.* J Phys Chem A, 2010. **114**(2): p. 879–83.
11. Chambreau, S.D., et al., *Heats of vaporization of room temperature ionic liquids by tunable vacuum ultraviolet photoionization.* J Phys Chem B, 2010. **114**(3): p. 1361–7.
12. Wang, C., et al., *Direct UV-spectroscopic measurement of selected ionic-liquid vapors.* Phys Chem Chem Phys, 2010. **12**(26): p. 7246–50.
13. Zaitsau, D., et al., *Experimental vapor pressures of 1-alkyl-3-methylimidazolium bis(trifluoromethylsulfonyl) imides and a correlation scheme for estimation of vaporization enthalpies of ionic liquids.* Journal of Physical Chemistry A, 2006. **110**: p. 7303–7306.
14. Samson, J.A. and D.L. Ederer, *Vacuum ultraviolet spectroscopy*. Vol. 32. 2000: Academic press.
15. Maniam, K.K. and S. Paul, *Progress in Electrodeposition of Zinc and Zinc Nickel Alloys Using Ionic Liquids.* Applied Sciences, 2020. **10**(15): p. 5321.
16. Rüther, T., et al., *Electrolytes for Lithium (Sodium) Batteries Based on Ionic Liquids: Highlighting the Key Role Played by the Anion.* Batteries & Supercaps, 2020. **3**(9): p. 793–827.
17. Yu, L., et al., *Ionic liquid combined with $NiCo_2O_4$/rGO enhances electrochemical oxygen sensing.* Talanta, 2020. **209**: p. 120515.
18. Kumarasinghe, K.D.M.S.P.K., et al., *Usage of Ionic Liquid Electrolyte in Tin and Zinc Oxide Composite Dye-sensitized Solar Cells.* Chemistry Letters, 2020. **49**(12): p. 1470–1472.
19. Zanchet, L., et al., *3-Triethylammonium propane sulfonate ionic liquids for Nafion-based composite membranes for PEM fuel cells.* Journal of Materials Science, 2020. **55**(16): p. 6928–6941.

20. Sosnowska, A., et al., *Relatively high-Seebeck thermoelectric cells containing ionic liquids supplemented by cobalt redox couple.* Journal of Molecular Liquids, 2020. **316**: p. 113871.
21. dos Santos Junior, G.A., et al., *High-Performance Lithium-Ion Hybrid Supercapacitors Based on Lithium Salt/Imidazolium Ionic Liquid Electrolytes and Ni-Doped $LiMn_2O_4$ Cathode Materials.* ACS Applied Energy Materials, 2020. **3**(9): p. 9028–9039.
22. Kondo, Y., T. Koyama, and S. Sasaki, *Tribological Properties of Ionic Liquids*, in *Ionic Liquids – New Aspects for the Future*. 2013, InTech.
23. Jia, H., et al., *Study of a gemini surface active ionic liquid 1,2-bis(3-hexylimidazolium-1-yl) ethane bromide as a high performance shale inhibitor and inhibition mechanism.* Journal of Molecular Liquids, 2020. **301**: p. 112401.
24. Zhou, L., et al., *Ionic Liquid-Dispersive Micro-Extraction and Detection by High Performance Liquid Chromatography–Mass Spectrometry for Antifouling Biocides in Water.* Molecules, 2023. **28**(3): p. 1263.
25. Morais, E.S., et al., *Use of Ionic Liquids and Deep Eutectic Solvents in Polysaccharides Dissolution and Extraction Processes towards Sustainable Biomass Valorization.* Molecules, 2020. **25**(16): p. 3652.
26. Ovejero-Pérez, A., et al., *Acidic depolymerization vs ionic liquid solubilization in lignin extraction from eucalyptus wood using the protic ionic liquid 1-methylimidazolium chloride.* International Journal of Biological Macromolecules, 2020. **157**: p. 461–469.
27. Bera, A., et al., *Recent advances in ionic liquids as alternative to surfactants/ chemicals for application in upstream oil industry.* Journal of Industrial and Engineering Chemistry, 2020. **82**: p. 17–30.
28. Patil, V., et al., *Synthesis of silver nanoparticles colloids in imidazolium halide ionic liquids and their antibacterial activities for gram-positive and gram-negative bacteria.* Chemosphere, 2020. **243**: p. 125302.
29. Brown, L., et al., *Ionic Liquid-Liquid Chromatography: A New General Purpose Separation Methodology.* Topics in Current Chemistry, 2017. **375**(5).
30. Pei, Y., et al., *Ionic liquids for advanced materials.* Materials Today Nano, 2022. **17**: p. 100159.
31. Tang, X., et al., *Recent development of ionic liquid-based electrolytes in lithium-ion batteries.* Journal of Power Sources, 2022. **542**: p. 231792.
32. Leones, R., et al., *Effect of the alkyl chain length of the ionic liquid anion on polymer electrolytes properties.* Electrochimica Acta, 2015. **184**: p. 171–178.
33. Kanai, K., et al., *Electronic structures of imidazolium-based ionic liquids.* Journal of Electron Spectroscopy and Related Phenomena, 2009. **174**(1): p. 110–115.
34. Gusain, R., et al., *Thermophysical properties of trioctylalkylammonium bis-(salicylato)borate ionic liquids: Effect of alkyl chain length.* Journal of Molecular Liquids, 2018. **269**: p. 540–546.
35. Cimini, A., et al., *Decomposition temperatures and vapour pressures of selected ionic liquids for electrochemical applications.* Journal of Thermal Analysis and Calorimetry, 2020. **142**(5): p. 1791–1797.
36. Deyko, A., et al., *The vapour of imidazolium-based ionic liquids: a mass spectrometry study.* Physical Chemistry Chemical Physics, 2011. **13**(37): p. 16841–16850.
37. Neto, B.A.D., et al., *Vapors from Ionic Liquids: Reconciling Simulations with Mass Spectrometric Data.* Journal of Physical Chemistry Letters, 2012. **3**(23): p. 3435–3441.

38. Armstrong, J.P., et al., *Vapourisation of ionic liquids.* Phys Chem Chem Phys, 2007. **9**(8): p. 982–90.
39. Leal, J.P., et al., *The nature of ionic liquids in the gas phase.* J Phys Chem A, 2007. **111**(28): p. 6176–82.
40. Gross, J.H., *Molecular ions of ionic liquids in the gas phase.* J Am Soc Mass Spectrom, 2008. **19**(9): p. 1347–52.
41. Kelkar, M.S. and E.J. Maginn, *Calculating the enthalpy of vaporization for ionic liquid clusters.* J Phys Chem B, 2007. **111**(32): p. 9424–7.
42. Koddermann, T., D. Paschek, and R. Ludwig, *Ionic liquids: dissecting the enthalpies of vaporization.* Chemphyschem, 2008. **9**(4): p. 549–55.
43. Ballone, P., et al., *Neutral and charged 1-butyl-3-methylimidazolium triflate clusters: equilibrium concentration in the vapor phase and thermal properties of nanometric droplets.* J Phys Chem B, 2007. **111**(18): p. 4938–50.
44. Koddermann, T., D. Paschek, and R. Ludwig, *Molecular dynamic simulations of ionic liquids: a reliable description of structure, thermodynamics and dynamics.* Chemphyschem, 2007. **8**(17): p. 2464–70.
45. Strasser, D., et al., *Tunable Wavelength Soft Photoionization of Ionic Liquid Vapors.* Journal of Physical Chemistry A, 2010. **114**(2): p. 879–883.
46. Lovelock, K.R., et al., *Vaporisation of a dicationic ionic liquid.* Chemphyschem, 2009. **10**(2): p. 337–40.
47. Weingarth, D., et al., *Electrochemical Stability of Imidazolium Based Ionic Liquids Containing Cyano Groups in the Anion: A Cyclic Voltammetry, XPS and DFT Study.* Journal of the Electrochemical Society, 2012. **159**(7): p. H611–H615.
48. Eftekhari, A., *Supercapacitors utilising ionic liquids.* Energy Storage Materials, 2017. **9**: p. 47–69.
49. Song, Y., et al., *In Situ Tracking of Organic Reactions at the Vapor/Liquid Interfaces of Ionic Liquids.* ChemPhysChem, 2018. **19**(20): p. 2741–2750.
50. Jia, M., A. Broderick, and J.T. Newberg, *The Influence of Water Vapor on the Electrochemical Shift of an Ionic Liquid Measured by Ambient Pressure X-ray Photoelectron Spectroscopy.* ChemPhysChem, 2021. **22**(7): p. 633–640.
51. Burba, C.M. and H.-C. Chang, *The Nature of Cation–Anion Interactions in Magnetic Ionic Liquids as Revealed Using High-Pressure Fourier Transform Infrared (FT-IR) Spectroscopy.* Applied Spectroscopy, 2019. **73**(5): p. 511–519.
52. Maniyarasu, S., et al., *Surface stability of ionic-liquid-passivated mixed-cation perovskite probed with in situ photoelectron spectroscopy.* Journal of Materials Chemistry A, 2022. **10**(35): p. 18206–18217.
53. Hozuki, N., et al., *Room-Temperature Preparation of Ta Ions-Containing Ionic Liquid and its Vapor Deposition toward Ta-Oxide Film Coating.* Journal of The Electrochemical Society, 2022. **169**(1): p. 013504.
54. Papović, S., et al., *Tutorial for thermal analysis of ionic liquids.* Journal of Thermal Analysis and Calorimetry, 2024. **149**(20): p. 11407–11419.
55. Miao, L., et al., *Ionic Liquids for Supercapacitive Energy Storage: A Mini-Review.* Energy & Fuels, 2021. **35**(10): p. 8443–8455.
56. Ilawe, N.V., et al., *Chemical and Radiation Stability of Ionic Liquids: A Computational Screening Study.* The Journal of Physical Chemistry C, 2016. **120**(49): p. 27757–27767.
57. Maiti, A., A. Kumar, and R.D. Rogers, *Water-clustering in hygroscopic ionic liquids—an implicit solvent analysis.* Physical Chemistry Chemical Physics, 2012. **14**(15): p. 5139.

58. Edmond de Hoffmann, V.S., *Mass Spectrometry. Principles and Applications*. Third ed. 2007. 489.
59. Kuusik, I., et al., *Near threshold photodissociation study of $EMIMBF_4$ vapor.* Rsc Advances, 2015. **5**(9): p. 6834–6842.
60. Berholts, M., *Fragmentation of ionic and hydrogen-bonded molecules induced by synchrotron radiation*. 2018, University of Tartu, University of Turku. p. 81.
61. Wiedemann, H., *Of Fields and Forces*, in *Particle Accelerator Physics*, H. Wiedemann, Editor. 2007, Springer Berlin Heidelberg: Berlin, Heidelberg. p. 3–35.
62. Kim, K.-J., *Synchrotron Radiation and Free-Electron Lasers*. 2017: Cambridge University Press.
63. Petersen, H., *The plane grating and elliptical mirror: A new optical configuration for monochromators.* Optics Communications, 1982. **40**(6): p. 402–406.
64. Riemer, F. and R. Torge, *Bessy SX 700 UHV monochromator: Design features and kinematic concept.* Nuclear Instruments and Methods in Physics Research, 1983. **208**(1–3): p. 313–314.
65. Follath, R. and F. Senf, *New plane-grating monochromators for third generation synchrotron radiation light sources.* Nuclear Instruments & Methods in Physics Research Section a-Accelerators Spectrometers Detectors and Associated Equipment, 1997. **390**(3): p. 388–394.
66. Parna, R., et al., *FinEstBeaMS – A wide-range Finnish-Estonian Beamline for Materials Science at the 1.5 GeV storage ring at the MAX IV Laboratory.* Nuclear Instruments & Methods in Physics Research Section a-Accelerators Spectrometers Detectors and Associated Equipment, 2017. **859**: p. 83–89.
67. Sasaki, S., et al., *Design of a new type of planar undulator for generating variably polarized radiation.* Nuclear Instruments and Methods in Physics Research Section A: Accelerators, Spectrometers, Detectors and Associated Equipment, 1993. **331**(1–3): p. 763–767.
68. *Modern Developments in X-ray and Neutron Optics*. Springer Series in Optical Sciences, ed. A. Erko, et al. 2008, Berlin: Springer.
69. Kooser, K., et al., *Gas-phase endstation of electron, ion and coincidence spectroscopies for diluted samples at the FinEstBeAMS beamline of the MAX IV 1.5 GeV storage ring.* Journal of Synchrotron Radiation, 2020. **27**(4): p. 1080–1091.
70. Wang, W., et al., *A new user-friendly materials science end station at the FinEstBeAMS beamline of MAX IV.* Journal of Physics: Conference Series, 2022. **2380**(1): p. 012048.
71. Pankratov, V., et al., *Progress in development of a new luminescence setup at the FinEstBeAMS beamline of the MAX IV laboratory.* Radiation Measurements, 2019. **121**: p. 91–98.
72. B.D., M., *A Handbook of Spectroscopic Data Chemistry (UV, IR, PMR, CNMR and Mass Spectroscopy)*. 2009: Oxford Book Company.
73. Bundaleski, N., et al., *Ion-induced fragmentation of imidazolium ionic liquids: TOF-SIMS study.* International Journal of Mass Spectrometry, 2013. **353**: p. 19–25.
74. Dunaev, A.M., et al., *Dimer neutral ion pairs and associative ions in saturated vapor of 1-ethyl-3-methylimidazolium trifluoromethanesulfonate ionic liquid.* Calphad, 2019. **65**: p. 127–131.
75. Regeta, K., et al., *Free electrons and ionic liquids: study of excited states by means of electron-energy loss spectroscopy and the density functional theory multi-reference configuration interaction method.* Physical Chemistry Chemical Physics, 2015. **17**(24): p. 15771–15780.

76. Chambreau, S.D., et al., *Thermal decomposition mechanisms of alkylimidazolium ionic liquids with cyano-functionalized anions.* J Phys Chem A, 2014. **118**(47): p. 11119–32.
77. Liu, J., S.D. Chambreau, and G.L. Vaghjiani, *Dynamics simulations and statistical modeling of thermal decomposition of 1-ethyl-3-methylimidazolium dicyanamide and 1-ethyl-2,3-dimethylimidazolium dicyanamide.* J Phys Chem A, 2014. **118**(47): p. 11133–44.
78. Hollóczki, O., et al., *Carbenes in ionic liquids.* New Journal of Chemistry, 2010. **34**(12): p. 3004.
79. Rodríguez, H., et al., *Reaction of elemental chalcogens with imidazolium acetates to yield imidazole-2-chalcogenones: direct evidence for ionic liquids as proto-carbenes.* Chemical Communications, 2011. **47**(11): p. 3222.
80. Navarro, P., et al., *Thermal Properties of Cyano-Based Ionic Liquids.* Journal of Chemical & Engineering Data, 2013. **58**(8): p. 2187–2193.
81. Tolstogouzov, A., et al., *Study on imidazolium-based ionic liquids with scanning atom probe and Knudsen effusion mass spectrometry.* Surface and Interface Analysis, 2008. **40**(13): p. 1614–1618.
82. Günster, J., et al., *A time-of-flight secondary ion mass spectroscopy study of 1-ethyl-3-methylimidazolium bis(trifluoromethylsulfonyl)imide RT-ionic liquid.* Surface Science, 2008. **602**(21): p. 3403–3407.
83. Souda, R., *Phase Transition of 1-Ethyl-3-Methylimidazolium Bis(trifluoro-methylsulfonyl)imide Thin Films on Highly Oriented Pyrolytic Graphite.* The Journal of Physical Chemistry B, 2009. **113**(39): p. 12973–12977.
84. Smith, E.F., et al., *Ionic Liquids in Vacuo: Analysis of Liquid Surfaces Using Ultra-High-Vacuum Techniques.* Langmuir, 2006. **22**(22): p. 9386–9392.
85. Moritani, K., et al., *Site-Specific Fragmentation of Polystyrene Molecule Using Size-Selected Ar Gas Cluster Ion Beam.* Applied Physics Express, 2009. **2**(4).
86. Lesimple, A., et al., *Electrospray mass spectral fragmentation study of N,N'-di-substituted imidazolium ionic liquids.* Journal of the American Society for Mass Spectrometry, 2006. **17**(1): p. 85–95.
87. Fogarty, R.M., et al., *Electron spectroscopy of ionic liquids: experimental identification of atomic orbital contributions to valence electronic structure.* Physical Chemistry Chemical Physics, 2019. **21**(35): p. 18893–18910.
88. Fogarty, R.M., et al., *Experimental validation of calculated atomic charges in ionic liquids.* The Journal of Chemical Physics, 2018. **148**(19): p. 193817.
89. Höfft, O., et al., *Electronic Structure of the Surface of the Ionic Liquid [EMIM][Tf_2N] Studied by Metastable Impact Electron Spectroscopy (MIES), UPS, and XPS.* Langmuir, 2006. **22**(17): p. 7120–7123.
90. Krischok, S., et al., *Surface structure of [XMIm]Tf_2N ultrathin ionic liquid films probed by metastable He atoms and photoelectron spectroscopies (UPS and XPS).* Nuclear Instruments & Methods in Physics Research Section B-Beam Interactions With Materials and Atoms, 2014. **340**: p. 51–57.
91. Asha, S., K.P. Vijayalakshmi, and B.K. George, *Pyrrolidinium-based ionic liquids as electrolytes for lithium batteries: A Computational Study.* International Journal of Quantum Chemistry, 2019. **119**(22).
92. Asha, S., K.P. Vijayalakshmi, and B.K. George, *Electronic structural studies of pyrrolidinium-based ionic liquids for electrochemical application.* International Journal of Quantum Chemistry, 2019. **119**(17).

93. Ong, S.P., et al., *Electrochemical Windows of Room-Temperature Ionic Liquids from Molecular Dynamics and Density Functional Theory Calculations.* Chemistry of Materials, 2011. **23**(11): p. 2979–2986.
94. Yildirim, H., et al., *Decomposition of Ionic Liquids at Lithium Interfaces. 1. Ab Initio Molecular Dynamics Simulations.* Journal of Physical Chemistry C, 2017. **121**(51): p. 28214–28234.
95. Haskins, J.B., C.W. Bauschlicher, and J.W. Lawson, *Ab Initio Simulations and Electronic Structure of Lithium-Doped Ionic Liquids: Structure, Transport, and Electrochemical Stability.* The Journal of Physical Chemistry B, 2015. **119**(46): p. 14705–14719.
96. Kuusik, I., et al., *Valence band photoelectron spectra of [EMIM][BF_4] ionic liquid vapor: Evidences of electronic relaxation.* Journal of Molecular Liquids, 2016. **223**: p. 939–942.
97. Kuusik, I., et al., *Valence electronic structure of [EMIM][BF_4] ionic liquid: photo-emission and DFT plus D study.* Rsc Advances, 2018. **8**(53): p. 30298–30304.
98. Kuusik, I., et al., *Valence electronic structure of [EMIM][$B(CN)_4$]: ion-pair vs. bulk description.* RSC Advances, 2019. **9**(57): p. 33140–33146.

PUBLICATIONS

CURRICULUM VITAE

Name	Mati Kook
Date of birth	02.01.1988
Researcher ID	Q-4461-2017
ORCID	0000-0002-1987-1792
E-mail	mati.kook@ut.ee

Additional information

Dedicated, independent, fast learner, great interest in new instrumentation and technologies.

Institutions and positions

20.12.2019–…	University of Tartu, Faculty of Science and Technology, Institute of Physics, University of Tartu, Laboratory Assistant
03.04.2019–19.12.2019	Visiting Researcher in MAX-IV Laboratory, Lund University, Lund, Sweden
01.04.2012–02.04.2019	University of Tartu, Faculty of Science and Technology, Institute of Physics, University of Tartu, Laboratory Assistant
2010–2011	Estonian Defence Forces, 11 months, driver training

Academic degrees

Mati Kook, Master's Degree, 2017, (sup) Vambola Kisand; Rainer Pärna; Ergo Nõmmiste, Süsinikmaterjalide ja galliumarseniidi röntgenfotoelektronspektroskoopilised uuringud (X-ray Photoelectron Spectroscopic Studies of Gallium Arsenide and Carbon Materials), University of Tartu, Faculty of Science and Technology, Institute of Physics

Mati Kook, PhD student, (sup) Rainer Pärna; Vambola Kisand; Ergo Nõmmiste, Photoexcited processes in gaseous ionic liquids and in ionic liquid/substrate interfaces, University of Tartu, Faculty of Science and Technology, Institute of Physics

Education

2008–... University of Tartu

2006–2008 Tartu Täiskasvanute Gymnasium

1995–2004 Tartu Annemõisa School

Publications

2024

Danilian, Dmytro; Bundruck, Franziska Maria; Kikas, Arvo; Kaambre, Tanel; Mandar, Hugo; Lehner, Sandro; Gogos, Alexander; Kozlova, Jekaterina; Kook, Mati; Kiisk, Valter; Link, Joosep; Stern, Raivo; Ivask, Angela; Kisand, Vambola; Parna, Rainer (2024). Reusable magnetic mixture of $CuFe_2O_4$-Fe_2O_3 and TiO_2 for photocatalytic degradation of pesticides in water. RSC Advances, 14 (18), 12337–12348. DOI: 10.1039/d4ra00094c.

Kuusik, Ivar; Kook, Mati; Käämbre, Tanel; Michailoudi, Georgia; Tõnisoo, Arvo; Kisand, Vambola; Pärna, Rainer (2024). Gas-phase PES and GW investigation of two widespread herbicides: MCPA and 2,4-dichlorophenoxyacetic acid. Journal of Electron Spectroscopy and Related Phenomena, 275, 147462-1–147462-4. DOI: 10.1016/j.elspec.2024.147462.

2023

Kaur, Harleen; Rosenberg, Merilin; Kook, Mati; Danilian, Dmytro; Kisand, Vambola; Ivask, Angela (2023). Antibacterial activity of solid surfaces is critically dependent on relative humidity, inoculum volume and organic soiling. FEMS Microbes, xtad022. DOI: 10.1093/femsmc/xtad022.

2022

Kook, Mati; Kuusik, Ivar; Parna, Rainer; Käämbre, Tanel; Kikas, Arvo; Tõnisoo, Arvo; Kahk, Juhan Matthias; Kivimäki, Antti; Reisberg, Liis; Kisand, Vambola (2022). Ion fragmentation study of [EMMIM][TFSI], [EMIM][OTf] and [EMIM] [DCA] by vacuum ultraviolet light. International Journal of Mass Spectrometry, 471, ARTN 116732. DOI: 10.1016/j.ijms.2021.116732.

Kisand, Vambola; Visnapuu, Meeri; Rosenberg, Merilin; Danilian, Dmytro; Vlassov, Sergei; Kook, Mati; Lange, Sven; Pärna, Rainer; Ivask, Angela (2022). Antimicrobial Activity of Commercial Photocatalytic SaniTise™ Window Glass. Catalysts, 12 (2), ARTN 197. DOI: 10.3390/catal12020197.

2021

Pelimanni, Eetu; Hautala, Lauri; Hans, Andreas; Kivimäki, Antti; Kook, Mati; Küstner-Wetekam, Catmarna; Marder, Lutz; Patanen, Minna; Huttula, Marko (2021). Core and Valence Level Photoelectron Spectroscopy of Nanosolvated KCl. The Journal of Physical Chemistry A, 4750–4759. DOI: 10.1021/acs.jpca.1c01539.

Juvanen, Silver; Sarapuu, Ave; Vlassov, Sergei; Kook, Mati; Kisand, Vambola; Kaarik, Maike; Treshchalov, Alexey; Aruvali, Jaan; Kozlova, Jekaterina; Tamm, Aile; Leis, Jaan; Tammeveski, Kaido (2021). Iron-Containing Nitrogen-Doped Carbon Nanomaterials Prepared via NaCl Template as Efficient Electrocatalysts for the Oxygen Reduction Reaction. ChemElectroChem, 8 (12), 2288–2297. DOI: 10.1002/celc.202100571.

Chernenko, Kirill; Kivimaki, Antti; Pärna, Rainer; Wang, Weimin; Sankari, Rami; Leandersson, Mats; Tarawneh, Hamed; Pankratov, Vladimir; Kook, Mati; Kukk, Edwin; Reisberg, Liis; Urpelainen, Samuli; Käämbre, Tanel; Siewert, Frank; Gwalt, Grzegorz; Sokolov, Andrey; Lemke, Stephanie; Alimov, Svyatoslav; Knedel, Jeniffa; Kutz, Oliver ... Huttula, Marko (2021). Performance and characterization of the FinEsuseAMS beamline at the MAX IV Laboratory. Journal of Synchrotron Radiation, 28, 1620–1630. DOI: 10.1107/S1600577521006032.

Kuusik, Ivar; Kook, Mati; Parna, Rainer; Kisand, Vambola (2021). Ionic Liquid Vapors in Vacuum: Possibility to Derive Anodic Stabilities from DFT and UPS. ACS Omega, 6 (8), 5255–5265. DOI: 10.1021/acsomega.0c05369.

Kruusma, Jaanus; Tonisoo, Arvo; Paerna, Rainer; Thomberg, Thomas; Kook, Mati; Romann, Tavo; Kisand, Vambola; Lust, Enn (2021). The Electrochemical Behaviour of Quaternary Amine-Based Room-Temperature Ionic Liquid N4111(TFSI). Catalysts, 11 (11), ARTN 1315. DOI: 10.3390/catal11111315.

Kruusma, Jaanus; Tonisoo, Arvo; Parna, Rainer; Thomberg, Thomas; Kook, Mati; Romann, Tavo; Kisand, Vambola; Lust, Enn (2021). The electrochemical behaviour of protic quaternary amine based room-temperature ionic liquid N2210(OTf) at negatively and positively polarized micro-mesoporous carbon electrode investigated by in situ X-ray photoelectron spectroscopy, in situ mass-spectroscopy, cyclic voltammetry and electrochemical impedance spectroscopy methods. Journal of Electroanalytical Chemistry, 897, ARTN 115561. DOI: 10.1016/j.jelechem.2021.115561.

2020

Ping, Kefeng; Braschinsky, Alan; Alam, Mahboob; Bhadoria, Rohit; Mikli, Valdek; Mere, Arvo; Aruväli, Jaan; Paiste, Päärn; Vlassov, Sergei; Kook, Mati; Rähn, Mihkel; Sammelselg, Väino; Tammeveski, Kaido; Kongi, adežda; Starkov, Pavel (2020). Fused hybrid linkers for metal–organic frameworks-derived bifunctional oxygen electrocatalysts. ACS Applied Energy Materials, 3 (1), 152–157. DOI: 10.1021/acsaem.9b02039.

Sibul, Roberta; Kibena-Põldsepp, Elo; Ratso, Sander; Kook, Mati; Sougrati, Moulay Tahar; Käärik, Maike; Merisalu, Maido; Aruväli, Jaan; Paiste, Päärn; Treshchalov, Alexey; Leis, Jaan; Kisand, Vambola; Sammelselg, Väino; Holdcroft, Steven; Jaouen, Frédéric; Tammeveski, Kaido (2020). Iron- and nitrogen-doped graphene-based catalysts for fuel cell applications. ChemElectroChem, 7 (7), 1739–1747. DOI: 10.1002/celc.202000011.

Teppor, Patrick; Jäger, Rutha; Härk, Eneli; Sepp, Silver; Kook, Mati; Volobujeva, Olga; Paiste, Päärn; Kochovski, Zdravko; Tallo, Indrek; Lust, Enn (2020). Exploring Different Synthesis Parameters for the Preparation of Metal-Nitrogen-Carbon Type Oxygen Reduction Catalysts. Journal of The Electrochemical Society, 167 (5), 054513. DOI: 10.1149/1945-7111/ab7093.

Kooser, Kuno; Käämbre, Tanel; Vestli, Mihkel; Joost, Urmas; Urpelainen, Samuli; Kook, Mati; Bournel, Fabrice; Gallet, Jean-Jacques; Lust, Enn; Kukk, Edwin; Nurk, Gunnar (2020). Operando high-temperature near-ambient pressure X-ray photoelectron spectroscopy and impedance spectroscopy study of Ni–$Ce_{0.9}Gd_{0.1}O_{2-\delta}$ solid oxide fuel cell anode. International Journal of Hydrogen Energy, 45, 25286–25298. DOI: 10.1016/j.ijhydene.2020.06.228.

2019

Šutka, Anna; Järvekülg, Martin; Gross, Karlis Agris; Kook, Mati; Käämbre, Tanel; Visnapuu, Meeri; Trefalt, Gregor; Šutka, Andris (2019). Visible Light to switch-on Desorption from Goethite. Nanoscale, 11, 3794–3798. DOI: 10.1039/C8NR09547G.

Praats, Reio; Kruusenberg, Ivar; Käärik, Maike; Joost, Urmas; Aruväli, Jaan; Paiste, Päärn; Saar, Rando; Rauwel, Protima; Kook, Mati; Leis, Jaan; Zagal, José H.; Tammeveski, Kaido (2019). Electroreduction of oxygen in alkaline solution on iron phthalocyanine modified carbide-derived carbons. Electrochimica Acta, 299, 999–1010. DOI: 10.1016/j.electacta.2019.01.062.

Silva, Thamires Canuto de Almeida e; Mooste, Marek; Kibena-Põldsepp, Elo; Matisen, Leonard; Merisalu, Maido; Kook, Mati; Sammelselg, Väino; Tammeveski, Kaido; Wilhelm, Michaela; Rezwan, Kurosch (2019). Polymer-derived Co/Ni-SiOC(N) ceramic electrocatalysts for oxygen reduction reaction in fuel cells. Catalysis Science & Technology, 9 (3), 854–866. DOI: 10.1039/c8cy02207k.

Ratso, Sander; Käärik, Maike; Kook, Mati; Paiste, Päärn; Aruväli, Jaan; Vlassov, Sergei; Kisand, Vambola; Leis, Jaan; Kannan, Arunachala M.; Tammeveski, Kaido (2019). High performance catalysts based on Fe/N co-doped carbide-derived carbon and carbon nanotube composites for oxygen reduction reaction in acid media. International Journal of Hydrogen Energy, 44 (25), 12636–12648. DOI: 10.1016/j.ijhydene.2018.11.080.

Mooste, Marek; Kibena-Põldsepp, Elo; Vassiljeva, Viktoria; Merisalu, Maido; Kook, Mati; Treshchalov, Alexey; Kisand, Vambola; Uibu, Mai; Krumme, Andres; Sammelselg, Väino; Tammeveski, Kaido (2019). Electrocatalysts for oxygen reduction reaction based on electrospun polyacrylonitrile, styrene–acrylonitrile copolymer and carbon nanotube composite fibres. Journal of Materials Science, 54 (17), 11618–11634. DOI: 10.1007/s10853-019-03725-z.

Zukuls, Anzelms; Eglītis, Raivis; Käämbre, Tanel; Kook, Mati; Kisand, Vambola; Maiorov, Mikhael; Ignatans, Reinis; Duarte, Roberto Félix; Järvekülg, Martin; Šutka, Andris (2019). Magnetic and optical properties in degenerated transition metal and Ga co-substituted ZnO nanocrystals. Journal of Alloys and Compounds, 805, 1191–1199.
DOI: 10.1016/j.jallcom.2019.07.197.

Kuusik, Ivar; Kook, Mati; Pärna, Rainer; Kivimäki, Antti; Käämbre, Tanel; Reisberg, Liis; Kikas, Arvo; Kisand, Vambola (2019). The electronic structure of ionic liquids based on the TFSI anion: A gas phase UPS and DFT study. Journal of Molecular Liquids, 294, ARTN 111580–111580-5. DOI: 10.1016/j.molliq.2019.111580.

Käärik, Maike; Arulepp, Mati; Kook, Mati; Kozlova, Jekaterina; Ritslaid, Peeter; Aruväli, Jaan; Mäeorg, Uno; Sammelselg, Väino; Leis, Jaan (2019). High-performance microporous carbon from deciduous wood-origin metal carbide. Microporous and Mesoporous Materials, 278, 14–22. DOI: 10.1016/j.micromeso.2018.11.010.

Hussain, Sajid; Erikson, Heiki; Kongi, Nadezda; Tarre, Aivar; Ritslaid, Peeter; Kook, Mati; Rähn, Mihkel; Merisalu, Maido; Sammelselg, Väino; Tammeveski, Kaido (2019). Improved ORR Activity and Long-Term Durability of Pt Nanoparticles Deposited on TiO2-Decorated Multiwall Carbon Nanotubes. Journal of The Electrochemical Society, 166 (16), F1284–F1291. DOI: 10.1149/2.0071916jes.

Nurk, Gunnar; Kooser, Kuno; Korjus, Ove; Kanarbik, Rait; Urpelainen, Samuli; Käämbre, Tanel; Joost, Urmas; Kook, Mati; Kodu, Margus; Möller, Priit; Kivi, Indrek; Vestli, Mihkel; Gallet, Jean-Jacques; Bournel, Fabrice; Kukk, Edwin; Lust, Enn; (2019). Operando NAP-HT-XPS and Impedance Spectroscopy Study of Pulsed Laser Deposited Ni-$Ce_{0.9}Gd_{0.1}O_{2-\delta}$ Solid Oxide Fuel Cell Electrode. In: K. Eguchi; S.C. Singhal (Ed.). ECS Transactions. (555–561). Solid Oxide Fuel Cells 16 (SOFC-XVI). United States of America: The Electrochemical Society. DOI: 10.1149/09101.0555ecst.

Teppor, Patrick; Jäger, Rutha; Härk, Eneli; Sepp, Silver; Volobujeva, Olga; Kook, Mati; Paiste, Päärn; Tallo, Indrek; Lust, Enn (2019). The influence of synthesis conditions to a facile Co-N/C type ORR catalyst synthesis method in RDE and fuel cell measurements. *Electrolysis and Fuel Cell Discussions 2019 – Towards Catalysts Free of Critical Raw Materials for Fuel Cells and Electrolysers: Electrolysis and Fuel Cell Discussions 2019 – Towards Catalysts Free of Critical Raw Materials for Fuel Cells and Electrolysers, La Grande Motte, France, 15th–18th September 2019.* EFCD2019, 38.

Mati Kook, Liis Reisberg, Ivar Kuusik, Marta Bernholts, Meeri Lembinen, Tanel Käämbre, Vambola Kisand, Arvo Kikas, Antti Kivimäki and Rainer Pärna (2019). The electronic structure of gas-phase 2-aminoterephthalic acid. In: 31st MAX IV User Meeting 31st MAX IV User Meeting, Scandic Star Lund (Glimmervägen 5, 224 78 Lund, Rootsi), 23–25 September 2019. UM19.

Ivar Kuusik, Mati Kook, Rainer Pärna, Antti Kivimäki, Tanel Käämbre, Liis Reisberg, Arvo Kikas, Vambola Kisand (2019). The electronic structure of ionic liquids: results from UPS and DFT studies. In: 31st MAX IV User Meeting 31st MAX IV User Meeting, Scandic Star Lund (Glimmervägen 5, 224 78 Lund, Rootsi), 23–25 September 2019. UM19.

2018

Käärik, Maike; Arulepp, Mati; Kook, Mati; Mäeorg, Uno; Kozlova, Jekaterina; Sammelselg, Väino; Perkson, Anti; Leis, Jaan (2018). Characterisation of steam-treated nanoporous carbide-derived carbon of TiC origin: structure and enhanced electrochemical performance. Journal of Porous Materials, 25 (4), 1057–1070. DOI: 10.1007/s10934-017-0517-8.

Ratso, Sander; Kruusenberg, Ivar; Käärik, Maike; Kook, Mati; Puust, Laurits; Saar, Rando; Leis, Jaan; Tammeveski, Kaido (2018). Highly efficient transition metal and nitrogen co-doped carbide-derived carbon electrocatalysts for anion exchange membrane fuel cells. Journal of Power Sources, 375, 233–243. DOI: 10.1016/j.jpowsour.2017.08.046.

Šutka, Andris; Käämbre, Tanel; Joost, Urmas; Kooser, Kuno; Kook, Mati; Duarte, Roberto Felix; Kisand, Vambola; Maiorov, Mikhael; Döbelin, Nicola; Smits, Krisjanis (2018). Solvothermal synthesis derived Co-Ga codoped ZnO diluted magnetic degenerated semiconductor nanocrystals. Journal of Alloys and Compounds, 763, 164–172. DOI: 10.1016/j.jallcom.2018.05.036.

Ratso, Sander; Kaarik, Maike; Kook, Mati; Paiste, Paarn; Kisand, Vambola; Vlassov, Sergei; Leis, Jaan; Tammeveski, Kaido (2018). Iron and Nitrogen Co-doped Carbide-Derived Carbon and Carbon Nanotube Composite Catalysts for Oxygen Reduction Reaction. ChemElectroChem, 5 (14), 1827–1836. DOI: 10.1002/celc.201800132.

Mooste, Marek; Kibena-Põldsepp, Elo; Matisen, Leonard; Merisalu, Maido; Kook, Mati; Kisand, Vambola; Vassiljeva, Viktoria; Krumme, Andres; Sammelselg, Väino; Tammeveski, Kaido (2018). Oxygen reduction on catalysts prepared by pyrolysis of electrospun styrene-acrylonitrile copolymer and multi-walled carbon nanotube composite fibres. Catalysis Letters, 148 (7), 1815–1826. DOI: 10.1007/s10562-018-2392-6.

Teppor, Patrick; Jäger, Rutha; Härk, Eneli; Tallo, Indrek; Joost, Urmas; Kook, Mati; Paiste, Päärn; Šmits,Krisjanis; Kirsimäe, Kalle; Lust, Enn (2018). ORR Activity and Stability of Co-N/C Catalysts Based on Silicon Carbide Derived Carbon and the Impact of Loading in Acidic Media. Journal of The Electrochemical Society, 165 (14), F1217–F1223. DOI: 10.1149/2.0961814jes.

Sibul, Roberta; Kibena-Põldsepp, Elo; Ratso, Sander; Kook, Mati; Käärik, Maike; Merisalu, Maido; Paiste, Päärn; Leis, Jaan; Sammelselg, Väino; Tammeveski, Kaido (2018). Nitrogen-doped carbon-based electrocatalysts synthesised by ball-milling. Electrochemistry Communications, 93, 39–43. DOI: 10.1016/j.elecom.2018.05.027.

Hussain, Sajid; Erikson, Heiki; Kongi, Nadezda; Treshchalov, Alexey; Rähn, Mihkel; Kook, Mati; Merisalu, Maido; Matisen, Leonard; Sammelselg, Väino; Tammeveski, Kaido (2018). Oxygen electroreduction on Pt nanoparticles deposited on reduced graphene oxide and N-doped reduced graphene oxide prepared by plasma-assisted synthesis in aqueous solution. ChemElectroChem, 5 (19), 2902–2911. DOI: 10.1002/celc.201800582.

Kisand, Kaarel; Sarapuu, Ave; Peikolainen, Anna-Liisa; Seemen, Helina; Kook, Mati; Käärik, Maike; Leis, Jaan; Sammelselg, Väino; Tammeveski, Kaido (2018). Oxygen Reduction on Fe- and Co-Containing Nitrogen-Doped Nanocarbons. ChemElectroChem, 5 (14), 2002–2009. DOI: 10.1002/celc.201800353.

Ratso, Sander; Ranjbar Sahraie, Nastaran; Sougrati, Moulay Tahar; Käärik, Maike; Kook, Mati; Saar, Rando; Paiste, Päärn; Jia, Qingying; Leis, Jaan; Mukerjee, Sanjeev; Jaouen, Frédéric; Tammeveski, Kaido (2018). Synthesis of highly-active Fe-N-C catalysts for PEMFC with carbide-derived carbons. Journal of Materials Chemistry A, 6 (30), 14663–14674. DOI: 10.1039/c8ta02325e.

Kook, Mati; Kuusik, Ivar; Kikas, Arvo; Käämbre, Tanel; Pärna, Rainer; Nõmmiste, Ergo; Kisand, Vambola (2018). XPS Studies of [EMIM][BF4] Ionic Liquid Films. *FMNT 2018 Book of Abstracts: 12th International Conference Functional Materials and Nanotechnologies (FM&NT)*.Ed. Grīnberga, Līga; Šarakovskis, Anatolijs;. Riga: Institute of Solid State Physics, University of Latvia, 238–238.

Käärik, Maike; Arulepp, Mati; Kook, Mati; Kozlova, Jekaterina; Ritslaid, Peeter; Aruväli, Jaan; Mäeorg, Uno; Sammelselg, Väino; Leis, Jaan (2018). A Microporous Carbide-Derived Carbon of Leaf-Wood Origin as an Electrode Material for the Electrical Double-Layer Capacitor. *7th Baltic Electrochemistry Conference: Finding New Inspiration, Tartu, Estonia, November 4–7, 2018.* University of Tartu Press.

2017

Sarapuu, Ave; Kreek, Kristiina; Kisand, Kaarel; Kook, Mati; Uibu, Mai; Koel, Mihkel; Tammeveski, Kaido (2017). Electrocatalysis of oxygen reduction by iron-containing nitrogen-doped carbon aerogels in alkaline solution. Electrochimica Acta, 230, 81–88. DOI: 10.1016/j.electacta.2017.01.157.

Ratso, Sander; Kruusenberg, Ivar; Käärik, Maike; Kook, Mati; Saar, Rando; Pärs, Martti; Leis, Jaan; Tammeveski, Kaido (2017). Highly efficient nitrogen-doped carbide-derived carbon materials for oxygen reduction reaction in alkaline media. Carbon, 113, 159–169. DOI: 10.1016/j.carbon.2016.11.037.

Kodu, Margus; Berholts, Artjom; Kahro, Tauno; Kook, Mati; Ritslaid, Peeter; Seemen, Helina; Avarmaa, Tea; Alles, Harry; Jaaniso, Raivo (2017). Graphene functionalised by laser-ablated V_2O_5 for a highly sensitive NH3 sensor. Beilstein Journal of Nanotechnology, 8, 571–578. DOI: 10.3762/bjnano.8.61.

Šutka, Andris; Döbelin, Nicola; Joost, Urmas; Smits, Krisjanis; Kisand, Vambola; Maiorov, Mihael; Kooser, Kuno; Kook, Mati; Duarte, Roberto Felix; Käämbre, Tanel (2017). Facile synthesis of magnetically separable $CoFe_2O_4$/Ag_2O/Ag_2CO_3 nanoheterostructures with high photocatalytic performance under visible light and enhanced stability against photodegradation. Journal of Environmental Chemical Engineering, 5, 3455–3462. DOI: 10.1016/j.jece.2017.07.009.

Ratso, Sander; Kruusenberg, Ivar; Käärik, Maike; Kook, Mati; Saar, Rando; Kanninen, Petri; Kallio, Tanja; Leis, Jaan; Tammeveski, Kaido (2017). Transition metal-nitrogen co-doped carbide-derived carbon catalysts for oxygen reduction reaction in alkaline direct methanol fuel cell. Applied Catalysis B Environmental, 219, 276–286.
DOI: 10.1016/j.apcatb.2017.07.036.

2016

Ratso, Sander; Kruusenberg, Ivar; Sarapuu, Ave; Kook, Mati; Rauwel, Protima; Saar, Rando; Aruväli, Jaan; Tammeveski, Kaido (2016). Electrocatalysis of oxygen reduction on iron- and cobalt-containing nitrogen-doped carbon nanotubes in acid media. Electrochimica Acta, 218, 303–310.
DOI: 10.1016/j.electacta.2016.09.119.

ELULOOKIRJELDUS

Nimi	Mati Kook
Sünniaeg	02.01.1988
Researcher ID	Q-4461-2017
ORCID	0000-0002-1987-1792
E-post	mati.kook@ut.ee

Lisainfo

Pühendunud, iseseisev, kiire õppija, suur huvi uute mõõteseadmete ja tehnoloogia vastu.

Töökohad ja ametid

20.12.2019–…	Tartu Ülikool, Loodus- ja tehnoloogiateaduskond, Tartu Ülikooli Füüsika Instituut, laborant
03.04.2019–19.12.2019	Külalisteadur MAX-IV Labor, Lundi Ülikool, Lund, Rootsi
01.04.2012–02.04.2019	Tartu Ülikool, Loodus- ja tehnoloogiateaduskond, Tartu Ülikooli Füüsika Instituut, laborant
2010–2011	Kaitsevägi, 11 kuud, autojuht (1,00)

Teaduskraadid

Mati Kook, magistrikraad, 2017, (juh) Vambola Kisand; Rainer Pärna; Ergo Nõmmiste, Süsinikmaterjalide ja galliumarseniidi röntgenfotoelektronspektroskoopilised uuringud, Tartu Ülikool, Loodus- ja täppisteaduste valdkond, füüsika instituut

Mati Kook, doktorant, (juh) Rainer Pärna; Vambola Kisand; Ergo Nõmmiste, Photoexcited processes in gaseous ionic liquids and in ionic liquid/substrate interfaces (Fotoergastatud protsessid gaasfaasilistes ioonvedelikes ning ioonvedelik/substraat siirdekihtidel), Tartu Ülikool, Loodus- ja täppisteaduste valdkond, füüsika instituut

Haridustee

2008–...	Tartu Ülikool
2006–2008	Tartu Täiskasvanute Gümnaasium
1995–2004	Tartu Annemõisa Kool

Teadusartiklid

Toodud välja lehekülgedel 115–121.

DISSERTATIONES SCIENTIAE MATERIALIS UNIVERSITATIS TARTUENSIS

1. **Martin Järvekülg**. Tubular microstructures by Hf-, Zr- and Ti-butoxide gel sheet rolling. Tartu, 2011, 112 p.
2. **Sergei Vlassov**. Investigation of nanoscale interactions and mechanical properties of nanostructures using quartz tuning fork based real-time measurements. Tartu, 2011, 171 p.
3. **Margus Kodu**. Pulsed Laser Deposition of Magnesium Oxide and Barium Ternary Oxides for Plasma Display Protective Layers. Tartu, 2011, 89 p.
4. **Rainer Pärna**. Surface studies of some oxide films. Tartu, 2011, 129 p.
5. **Jevgeni Šulga**. Self-assembly and interaction of nanostructures. Tartu, 2011, 114 p.
6. **Wojciech Kuznik**. Quantum-chemical computer simulations of the linear and non-linear optical properties of pyrazoloquinoline and dicyanopyrazine derivatives. Tartu, 2012, 89 p.
7. **Leonid Dorogin**. Structural and tribological properties of zero- and one-dimensional nanocrystals. Tartu, 2012, 193 p.
8. **Viljar Palmre**. Fabrication and characterization of microporous carbon-based electroactive polymer actuators. Tartu, 2012, 99 p.
9. **Madis Paalo**. Synthesis of CNT-metal oxide nanocomposites: sol-gel process, rheology, structural and functional properties. Tartu, 2014, 175 p.
10. **Raul Välbe**. Developement of ionic liquid composites by sol-gel method for elaboration of industrial nano- and microstructures. Tartu, 2014, 97 p.
11. **Urmas Joost**. Impurity and preparation dependent properties of titania thin films. Tartu, 2014, 155 p.
12. **Madis Umalas**. Application of sol-gel technology for production of ceramic nanocomposites and functional coatings. Tartu, 2015, 136 p.
13. **Elena Samsonova**. Energy transfer probe as a tool to study morphological and structural origins of fluorescence quenching in rare-earth doped nanophosphors. Tartu, 2015, 114 p.
14. **Jay Mondal**. Novel Corrosion Protective Nanostructured Composite Coatings. Tartu, 2016, 104 p.
15. **Kathriin Utt**. Metal oxide mesostructures for optical applications. Tartu, 2016, 88 p.
16. **Kaido Siimon**. Electrospun gelatin cross-linked by glucose. Tartu, 2016, 84 p.
17. **Marko Part**. Combined three-dimensional sol-gel structures and atomic layer deposited thin films. Tartu, 2017, 162 p.
18. **Pejman Rasti**. Analysis of Remote Sensing Image Super Resolution using Fluid Lenses. Tartu, 2017, 188 p.
19. **Ivo Romet**. Recombination luminescence of doped borates: origin and application prospects in dosimetry. Tartu, 2017, 111 p.

20. **Vladimir I. Kondratiev**. Processing and characterization of transparent electrode materials. Tartu, 2017, 111 p.
21. **Taivo Jõgiaas**. Mechanical properties of atomic layer deposited thin films and nanocomposites. Tartu, 2017, 125 p.
22. **Lauri Aarik**. Atomic layer deposition and characterization of thin oxide films for application in protective coatings. Tartu, 2017, 180 p.
23. **Triin Kangur**. Preparation and functional properties of stochastic micro-structured sol-gel silica materials. Tartu, 2018, 96 p.
24. **Marta Berholts**. Fragmentation of ionic and hydrogen-bonded molecules induced by synchrotron radiation. Tartu, 2018, 126 p.
25. **Priit Priimägi**. Development and optimization of 3D-microbatteries. Tartu, 2018, 118 p.
26. **Siim Hödemann**. Residual stress determination in chemically strengthened and thermally tempered glass plates using scattered light method. Tartu, 2019, 146 p.
27. **Jekaterina Kozlova**. Complex characterization of graphene structures on nanometer level. Tartu, 2019, 206 p.
28. **Kristjan Kalam**. Magnetic, electric and structural properties of atomic layer deposited zirconia-based nanolaminates and mixtures. Tartu, 2020, 94 p.
29. **Triinu Vihmann**. Ionic liquids: synthesis and application in lubrication and lithography. Tartu, 2020, 102 p.
30. **Helina Seemen**. Atomic layer deposition and microscopic analysis of magnetically and electrically polarizable thin solid films. Tartu, 2021, 126 p.
31. **Ekaterina Vagapova**. Fluorescence quenching in inorganic crystalline solids activated by neodymium ions; from bulk to micro- and nanocrystals. Tartu, 2021, 116 p.
32. **Evgenii Strugovshchikov**. First-principles studies on rare-earth metal-hydride-based smart materials. Tartu, 2021, 166 p.
33. **Maido Merisalu**. Nanostructured Coatings for Car and Aerospace Industries. Tartu, 2022, 179 p.
34. **Elena Vinogradova**. Optical centers and quantum entangled states of Nd3+ ions in doped fluoride crystals. Tartu, 2023, 92 p.
35. **Dmytro Danilian**. “Photocatalytic materials for water treatment and antimicrobial applications”. Tartu, 2024, 139 p.
36. **Kristel Möls**. Metastable TiO_2-II in atomic layer deposited thin and ultrathin films: stabilization, properties and impact on film growth. Tartu, 2024, 112 p.
37. **Helle-Mai Piirsoo**. Mechanical Properties of Nanocomposites with Artificial Periodic Structure. Tartu, 2024, 144 p.
38. **Artjom Berholts**. Light-enhanced sensors of oxidizing gases based on single-layer CVD graphene. Tartu, 2024, 97 p.
39. **Alexandra Nefedova**. Oxide nanostructures as antiviral coatings for textiles. Tartu, 2025, 133 p.